CHALMERS

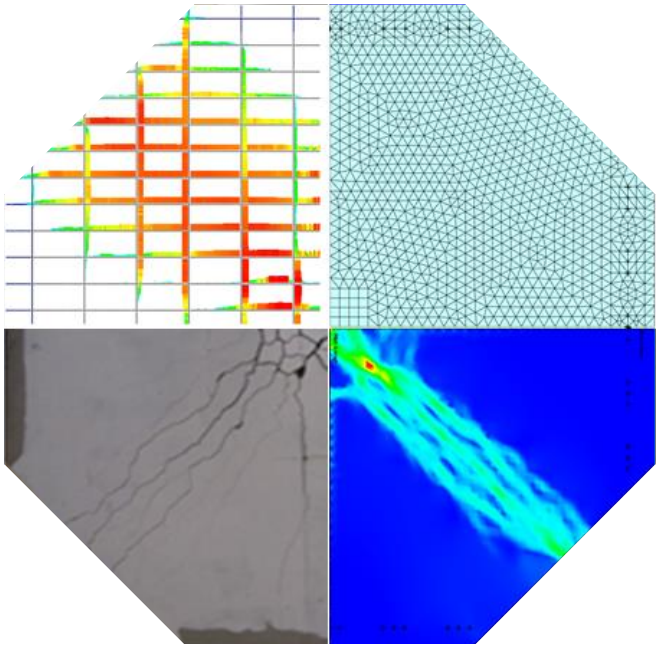

Finite element analysis of conventional and fiber reinforced concrete slabs

Master of Science Thesis in the Master's Programme Structural Engineering and Building Technology

FARSHID IRANI
BEHRANG MAZHARI ABADI

Department of Civil and Environmental Engineering
Division of Structural Engineering
Concrete Structures
CHALMERS UNIVERSITY OF TECHNOLOGY
Göteborg, Sweden 2013
Master's Thesis 2013:141

MASTER'S THESIS 2013:141

Finite element analysis of conventional and fiber reinforced concrete slabs

Master of Science Thesis in Master's programme Structural Engineering and building technology

FARSHID IRANI

BEHRANG MAZHARI ABADI

Department of Civil and Environmental Engineering
Division of Structural Engineering
Concrete Structures
CHALMERS UNIVERSITY OF TECHNOLOGY
Göteborg, Sweden 2013

Finite element analysis of conventional and fiber reinforced concrete slabs

Master of Science Thesis in the Master's Programme Structural Engineering and Building Technology

FARSHID IRANI
BEHRANG MAZHARI ABADI

Examensarbete / Institutionen för bygg- och miljöteknik,
Chalmers tekniska högskola 2013:141

Department of Civil and Environmental Engineering
Division of Structural Engineering
Concrete Structures
Chalmers University of Technology
SE-412 96 Göteborg
Sweden
Telephone: + 46 (0)31-772 1000

Cover:
Top left: Fully developed yield pattern for reinforcement
Top right: Triangular mesh
Bottom left: Crack pattern in the experiment
Bottom right: Crack pattern in FE analysis

Chalmers Reproservice / Department of Civil and Environmental Engineering
Göteborg, Sweden 2013

Finite element analysis of conventional and fiber reinforced concrete slabs

FARSHID IRANI
BEHRANG MAZHARI ABADI
Department of Civil and Environmental Engineering
Division of Structural Engineering
Concrete Structures
Chalmers University of Technology

ABSTRACT

Non-linear finite element analysis (FEA) is one of the leading tools to assess reinforced concrete structures. The aim of this project was to investigate how the behavior of reinforced concrete slabs can be described with FEA, and more specifically to investigate how different modeling choices affect the results in different load levels; i.e., from the beginning of the load application until a collapse mechanism is formed (failure). Non-linear FE analyses were performed, using the program DIANA, on two-way octagonal concrete slabs, which were simply supported along four edges and were subjected to a concentrated load in the middle. Three different configurations of reinforcement were considered: Conventional reinforcement , steel fiber reinforcement and a combination of both. The amount of steel bars in the slabs varied in the different directions; thus, the slabs had a strong and a weak direction. The analysis results were compared to experimental results from an ongoing research project.

The analyses were carried out using 2D curved shell elements and assuming full interaction between reinforcement and concrete. The concrete was modeled using constant and multi-linear models for compression and tension behavior respectively. Displacement control was used in static analyses, with Secant method for iterations.

To examine the effect of different modeling choices, a conventionally reinforced slab was considered as a reference model, and varying of modeling alternatives were executed in this model. The alternatives studied were: mesh (type, alignment and density), Poisson's ratio, crack band width, integration schemes, load application, input for material models and modeling of supports, addition of fibers, and the use of fibers as only reinforcement.

Two cases were studied for the mesh density: with a constant crack band width, and also when the crack band width was equal to the element size. In the first case, similar results were achieved by changing mesh densities while by having a crack band width equal to the element size, results showed that increasing the mesh density, more accurate results on the cracking point and less capacity from the yielding point until failure were obtained compared to the experiments. Thus, crack band width had a very important role in the study of mesh density.

Increasing Poisson's ratio did not affect the results before cracking, while lower stiffness and less capacity was observed in the post cracking stage until failure. When the crack band width was chosen as equal as the element size, the results agreed better to the experimental behavior in all loading stages, compared to when the crack band width was chosen to an assumed crack distance. In analyses with the same element size but smaller crack band width, significantly stiffer behavior in the cracking phase was obtained; however, less capacity was obtained from the yielding stage until failure. Very similar results were obtained in FE analyses for tensile models with multi-linear, exponential, linear and Hordijk softening. In the FE analysis of slabs with steel fiber reinforcement only, higher capacity and stiffer behavior were obtained compared to experimental results. For the slabs with combined steel fiber and conventional reinforcement, the cracking load was larger while the load from yielding until failure was lower in the analysis than in the experiments.

Key words: Non-linear analysis, DIANA, conventional reinforced slabs, steel fiber reinforced slabs (SFRC), modeling choices, parameter study

Contents

Preface

This study was carried out from January 2013 to October 2013, at the department of Civil and Environmental Engineering at Chalmers University of Technology. Students Farshid Irani and Behrang Mazhari Abadi were collaborating to accomplish this work.

This master thesis was related to the research project TailorCrete, funded by the European Community´s Seventh Framework Programme under agreement NMP2-LA-2009-228663. For more information regarding to TailorCrete please refer to: www.tailorcrete.com.

We would like to express our sincere appreciation to our supervisor David Fall and our examiner, Karin Lundgren at Chalmers for their patience and invaluable support throughout this study. Our genuine gratitude goes to our families for all their love and support over the years and for encouraging and supporting us in our studies.

Notations

Greeks

ε	Strain
$\emptyset_s$	Diameter of each steel bar
$\emptyset_f$	Diameter of each steel fiber
φ_x	Rotation around the *x*-axis
φ_y	Rotation around the *y*-axis
σ	Stress
ρ_s	Density of steel
ρ_c	Density of concrete
u_x	Translation about the *x*- axis
u_y	Translation about the *y*- axis
u_z	Translation about the *z*- axis
ν	Poison ratio
ΔF	Increment of load
ΔM	Increment of bending moment

Roman upper case letters

E_c	Young's modulus of concrete
E_s	Young's modulus of steel
E_{sf}	Young's modulus of steel fibers

F	Applied load
G_f	Fracture energy
M	Applied moment
V_f	Volume fraction

Roman lower case letters

f_{ck}	Characteristic compressive strength for concrete
f_{ct}	Tensile strength for concrete
f_{ft}	Tensile strength for fiber
f_u	Reinforcement ultimate strength
f_y	Reinforcement yield strength
h	Thickness of the concrete
h_{cr}	Crack band width
l_f	Length of each steel fiber
w	Crack opening

1 Introduction

1.1 Background

Concrete is one of the most ancient materials used in structures and became popular due to high compressive strength. To compensate the weakness of concrete in tension, steel bars were applied in tensile regions. Therefore, reinforced concrete (RC) was introduced in mid-1800s and it proved to be a revolutionary innovation in building structures, and over time, it became one of the most common materials in use.

The behavior of reinforced concrete before cracking is linear which makes the analysis of a structure simple. However, already for a small load, the non-linear behavior of RC makes it difficult to predict the response of the structure. Hence, non-linear finite element method can be a useful tool. The first published works dealing with nonlinear finite element analysis of concrete systems emerged in the late 1960s. These studies focused on various aspects of element formulation, including crack propagation and the bonding of reinforcement. Later on, much research has been conducted concerning the general application of finite element analyses to reinforced concrete.

1.2 Aim

The aim of this project was to investigate how the behavior of reinforced concrete slabs can be described in FEA, and more specifically to investigate how different modeling choices affect the results in different load levels; i.e., from the beginning of the load application until a collapse mechanism is formed (failure). Different modeling choices such as, modeling of supports, mesh (type, alignment, density), Poisson's ratio, load application, crack band width, integration scheme, material model, addition of fibers, and the use of fibers as only reinforcement were examined in FE analyses to investigate the effect of them.

1.3 Method

Non-linear analysis was performed by the use of a commercial FEM program, DIANA, and the results such as load versus displacement, crack pattern, support reactions etc. were compared with experimental data. Results from experiments recently carried out on octagonal concrete slabs (Fall, Rempling, & Lundgren, 2013), were used for comparison with the numerical analyses.

Slabs with three different reinforcement types were analyzed:

- Conventional reinforcement
- Steel fiber reinforcement
- Combination of both conventional and steel fiber reinforcement

1.4 Limitations

- Only curved shell elements were used in the modeling process.
- Only the reinforcement configurations in the chosen tests were modeled.
- An average value was used for the thickness of the slabs.
- All of the variation in parameters, such as Poisson's ratio, integration point, etc. was applied only in analyses of slabs with conventional reinforcement only.

1.5 Outline of the thesis

The thesis is organized in the following chapters:

Chapter 1 gives a general background to the work: the aim, scope and limitations

Chapter 2 presents a literature study, focusing on different type of reinforcement and finite element analyses.

Chapter 3 describes the modeled experiments: the test setup, material properties and how they affect the structural behavior.

Chapter 4 presents the different types of finite element models used.

Chapter 5 presents the results of FE analysis and effects of various modeling techniques are discussed.

Chapter 6 summarizes the significant results of the study and presents the conclusions.

2 Literature Survey

2.1 Reinforced concrete slabs

The load carrying of slabs can be in one or two directions. In one-way slabs load transfers to the supports along only one direction while in two-way slabs, the load is distributed in both main directions. The portion of the loads that each support will carry is governed by load-dividing lines which indicate the lines with zero shear force (Ericsson, 2010).

The main principle regarding design of slabs, is the use of sectional forces. Equilibrium conditions should be fulfilled in order to get the sectional forces in each direction. It should be mentioned that with varying amount of reinforcement in different directions, also the stiffness in the different directions will vary.

According to the Eurocode 2 (CEN, 2004), four different options exist to get the sectional forces:

- Linear static analysis: When the slab is assumed to be homogenous and distribution of the moments will be constant by increasing the load.
- Linear elastic analysis with limited redistribution: This is used for slabs with continuous strips. In the first step, linear analysis gives the moment distribution and in the second step, plastic redistribution between span and support moment modifies the moment distribution from the linear analysis.
- Plastic analysis: Two methods could be considered in this analysis type: lower bound approach and upper bound approach. For the results on the safe side, strip method is used which represents the lower bound approach and yield line method represents the upper bound approach (unsafe side).
- Non-linear analysis: This method provides full information of the structural behavior in all the load application but requires a lot of information from the early stage; hence it is not convenient to use as a design method.

2.2 Fiber reinforced concrete

2.2.1 Introduction

Fibers have been used as reinforcement since ancient times. Historically, horsehair was used in mortar and straw in mud bricks. Fiber reinforced concrete (FRC) is a mixture of Portland cement concrete reinforced with randomly distributed fibers while casting the concrete. The amount of fibers added to a concrete mix is expressed as a percentage of the total volume of the composite (concrete and fibers), termed "volume fraction" (V_f) which typically ranges from 0.1 to 3%. The effects of fibers depend on several parameters such as type, size, volume fraction and properties of fiber (Glavind, 1992). Different materials like steel, glass, synthetic or natural materials can be used as fibers and parameters such as weight, diameter, Young's modulus and tensile strength should be taken into consideration to choose the proper fiber (Daniel, 1998). Most commonly used in structures is a steel fiber, which was patented in 1874 by A. Berard. Both strain hardening and strain softening behavior of concrete can be obtained in steel fiber reinforced concrete (SFRC). Strain hardening behavior for SFRC is only possible if enough fibers are used (Jansson, 2011).

2.2.2 Effects of fibers on the structures

Fiber reinforced concrete offers the possibility to improve crack control (reduce crack width). It could also reduce the amount of steel bars and increase the flexural strength and durability (Jansson, 2008). In addition, fibers have a positive effect on the post peak ductility performance, fatigue strength, impact strength and reduce both shrinkage and temperature cracks (Bayasi, 1989). The way that fibers are oriented in the concrete has large impact on the FRC efficiency meaning that, suitable fiber orientation improves the tensile behavior of the structure (Grünewald, 2011).

2.2.3 Behavior of fibers on the structure

The tensile behavior of FRC can be classified as strain softening or strain hardening. When there is a localized single crack, the post-peak behavior will be strain softening; thus after cracking the stresses will decrease (Löfgren, 2005).

Figure 2.1 shows that fibers do not have any significant influence before first crack but have a favorable effect on the post cracking behavior of the structure; therefore it is more common to use fiber as secondary reinforcement.

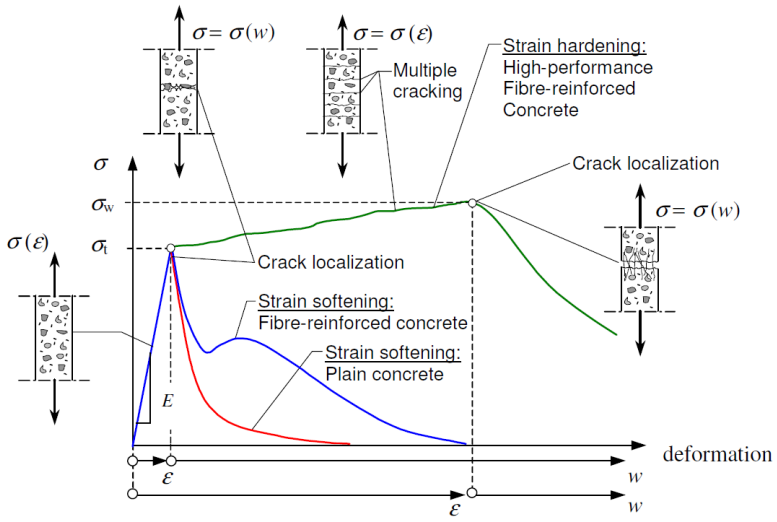

Figure 2.1 Difference in tensile behavior of cement-based materials, from (Löfgren, 2005).

2.3 Finite Element Method

A useful numerical tool for engineers is finite element method (FEM). The main reason why this approach is more convenient comparing to the other methods is that the geometry can be modeled for structures with any dimensions with regular and irregular shapes and there is no limitation for modeling different materials. Supports or restraints can be defined like their applied sources such as pressure, forces, etc. In order to solve the matrix equations, FEM uses standard process to governing differential equations and converting energy principles. In linear problems, the process can be performed fast with high accuracy.

In the post-processing, contour plots and diagrams can be created. Furthermore, errors can be estimated from second post-processing of derivatives, which helps the user to fix the defects and get more accurate results (Akin, 2009).

2.3.1 Non-linear FEM analysis

When structures have non-linear behavior, either due to material or geometrical effect, non-linear method can be used as a solution (Plos, 1996). There were two main problems in the early years of using this method: the first one was increasing need for computational time, which was reduced by the development of high-speed digital computers. The second factor was the complexity of non-linear analysis, which was solved by improving element characteristics and useful non-linear solution algorithms (Kwak, 1990).

In non-linear FEA, to determine static problems, an incremental iterative solution method is used. This solution acts in a step-wise manner and iterative procedure gives the result for each step increment. By increasing the load, loading history can be obtained by relation between each step.

The incrementation in incremental iterative solution method can be performed by three different methods (Plos, 1996):

- Load control: The load (Δf) is increased by incrementation process.
- Displacement control: The displacement (Δu) increases step by step, see Figure 2.2.
- Arc-length control: In this method, a control parameter is used instead of load or displacement as incrementation.

Combination of the mentioned methods cannot be used for the same step (Broo, Et al, 2008).

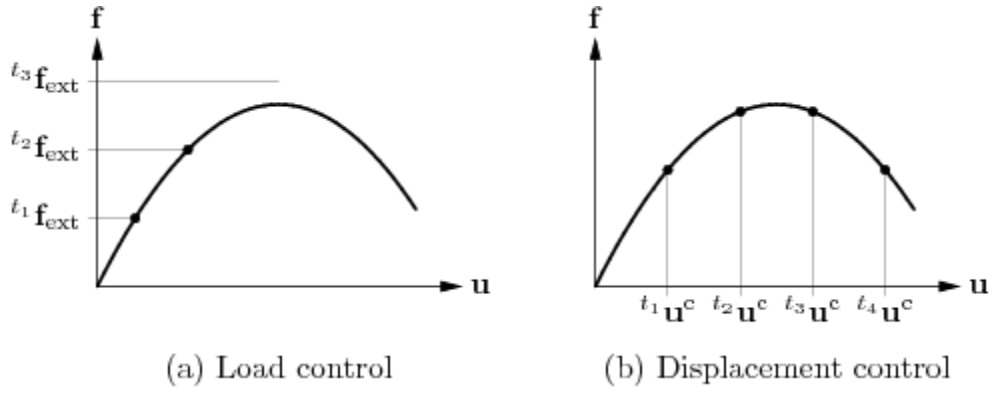

Figure 2.2 Load and displacement control, from (TNO Diana, 2009).

In all of the mentioned approaches, an iterative method is needed to reach equilibrium in load-displacement diagram. An initial stiffness is considered for iterative methods in the beginning and iteration will continue until convergence is reached which gives a new equilibrium point. Different iteration methods can be performed for iterative solution of each step (Plos, 1996):

- Regular Newton-Raphson where for each iteration, the stiffness matrix will be updated. This method is the most common one, see Figure 2.3(a).
- Modified Newton-Raphson where for each step, the stiffness matrix will be updated only once. Generally, this method leads to fewer numerical convergence problems. More iterations and less work is needed in each iteration, see Figure 2.3(b).
- Quasi Newton-Raphson method (also called Secant method) which performs an approximate way to update the inverse of the stiffness matrix to obtain a better convergence. This method was chosen for the iterations in this work, see Figure 2.3(c).

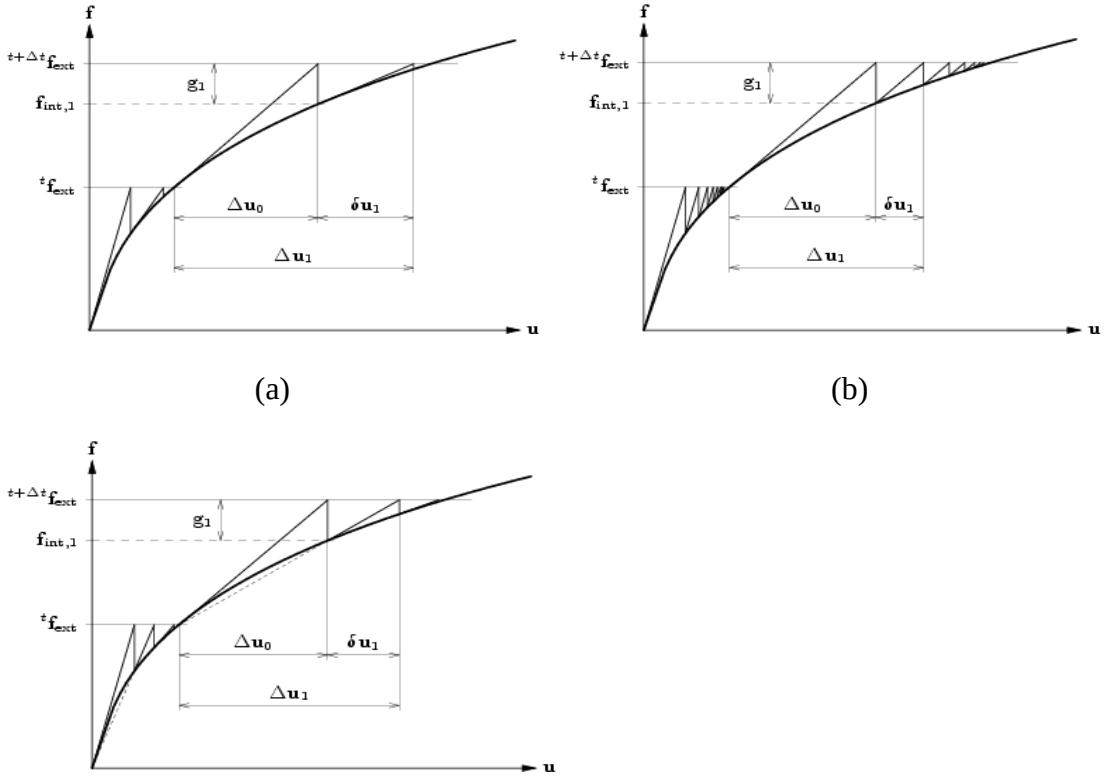

Figure 2.3 Iteration methods, a) Regular Newton-Raphson, b) Modified Newton-Raphson, c) Quasi Newton-Raphson, from (TNO Diana, 2009)

2.3.2 Concepts in Finite Element Material Modeling

- **Shell elements**

Shell elements are three-dimensional structures, made by combination of plane stress elements (membrane) and plate bending elements. In these structures the thickness is smaller than the other two dimensions and the direction of the load (*F*) can vary from perpendicular to the plane, to in-plane, and also the moment (*M*) has to be considered in-plane of the element. This type of element is very useful for modeling curved structures, because it leads to more accurate results (Cook, Malkus, & Plesha, 1989).

General shell elements can be classified as four different types; flat shell element, curved shell element, axisymmetric shell element and Mindlin type degenerated solid elements (Yang, Saigal, & Liaw, 1990). In addition to this, the thickness of the shell could also be used for classification of elements, i.e. thin shell element and thick shell element.

In this thesis, curved shell elements were chosen, see Figure 2.4.

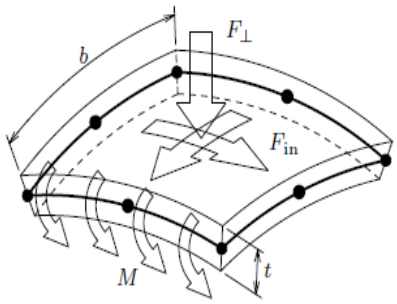

Figure 2.4 Curved shell elements, from (TNO Diana, 2009).

Some advantages of curved shell elements are:

- These elements are capable of modeling the coupling membrane-bending forces. In flat shell elements, these forces are independent from each other (Kansarav, 2004).
- They are compatible with embedded reinforcement in Diana and give better convergence in aspect of displacements and stresses (Plos, 1996).
- The thickness can vary along the element.

The geometry of the shell elements is made up by nodal point coordinates which are located in mid-surface. Each node has five degrees of freedom (DOF), three translations (u_x,u_y u_z) and two rotations (φ_x,φ_y), see Figure 2.5.

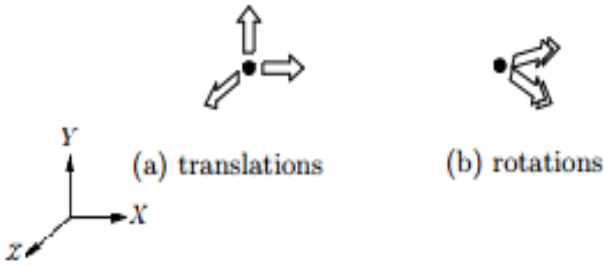

Figure 2.5 DOF in shell nodes, from (TNO Diana, 2009).

- **Embedded reinforcement**

In embedded reinforcement, full interaction between reinforcement and concrete is assumed. The elements are strengthened in the reinforcement direction with the same DOF as concrete. The displacement of concrete results in reinforcement strains which implies perfect bond between reinforcement and the surrounding material. The forces in each node correspond to the load acting on concrete and reinforcement. Finite element modeling using embedded method allows that the geometry of the reinforcement differs from the mesh geometry, which makes the user capable of generating a mesh without considering the location of the reinforcement in the mother elements.

There are two ways to model the embedded reinforcement in DIANA: bars and grids. In this thesis work bars were used. In order to model the bars in DIANA, three inputs should be defined by the user: material properties, the area of the cross section and the integration scheme. The topology and stresses in bar reinforcement method is shown in Figure 2.6.

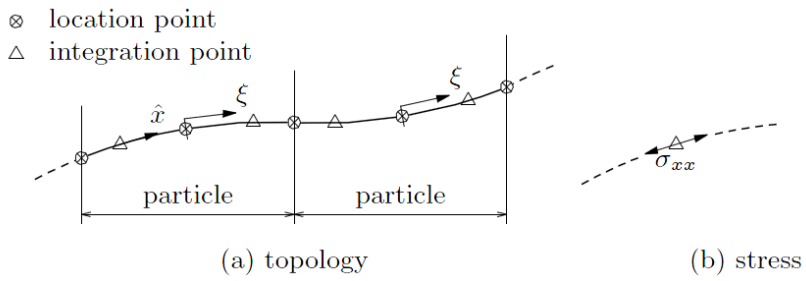

Figure 2.6 Topology and stresses in bar reinforcement, from (TNO Diana, 2009).

2.3.3 Modeling of the crack

Cracking of concrete is one of the parameters that should be taken into consideration in failure mechanism. In order to model the cracks, fracture energy (G_f), is defined as the energy needed to completely break a unit area of a material, see Figure 2.7.

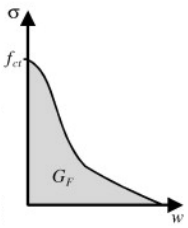

Figure 2.7 Fracture energy

There are three approaches to model the cracking in the concrete:

- Discrete crack approach
- Smeared crack approach
- Embedded crack approach

In discrete crack approach, the location of the crack has to be known in advance. Cracking is modeled by means of a displacement discontinuity at the interface between concrete elements. The cracked sections are modeled by separate crack elements and modeling of the rest of the elements which are in the uncracked regions is modeled by ordinary continuum elements.

A smeared crack model is used in this study to model cracking of concrete. In this approach, the material is assumed to be a continuum and the effect of cracking is described by means of an appropriate tensile stress-strain relationship (σ-ε). There is no individual crack and the model only represents the cracked region; the crack openings are smeared over the elements and represent the crack strains. This method is more convenient to use compared to discrete crack approach since there is no need to have full information about the crack such as crack type, special element, location and direction of the crack in advance. In the FE analyses carried out in this work, the smeared crack approach with a total strain crack model was used as the constitutive model. In this model, the tensile and compressive behavior of a material is described with uniaxial stress-strain relationship. The modeling of tensile and compressive behavior of the concrete is explained in the following, and the results of different analyses are discussed in Chapter 4.

- **Tension**

In the total strain crack model, there are two main curves to model the tensile behavior of concrete:

- Tensile curves which are not directly based on the fracture energy: elastic tensile behavior, constant tensile behavior, multi-linear behavior, brittle behavior and finally a general user-supplied subroutine. In this work, a multi-linear user defined stress-strain diagram was used for modeling the tensile behavior of the concrete, see Figure 2.8 (a, b, c and g).
- Tensile curves, which are directly based on the fracture energy: four softening functions are implemented in this category; a linear softening curve, exponential softening curve, nonlinear softening curve according to Reinhardt et al. and nonlinear softening curve according to Hordijk, see Figure 2.8 (d, e and f).

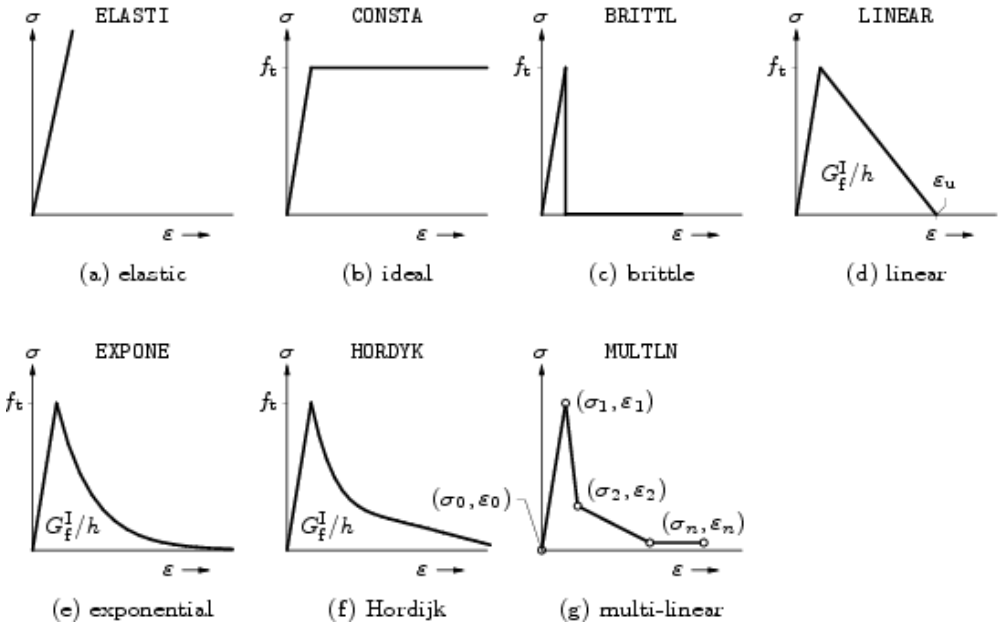

Figure 2.8 Tensile behavior for total strain crack model, from (TNO Diana, 2009).

- **Compression**

In general, the compressive behavior of the total strain crack model is a nonlinear function between uniaxial stress and strain. Different curves to describe the compressive behavior of the concrete are illustrated in Figure 2.9.

In this work, an ideal compression curve (constant) was chosen as compression model; see Figure 2.9 (b).

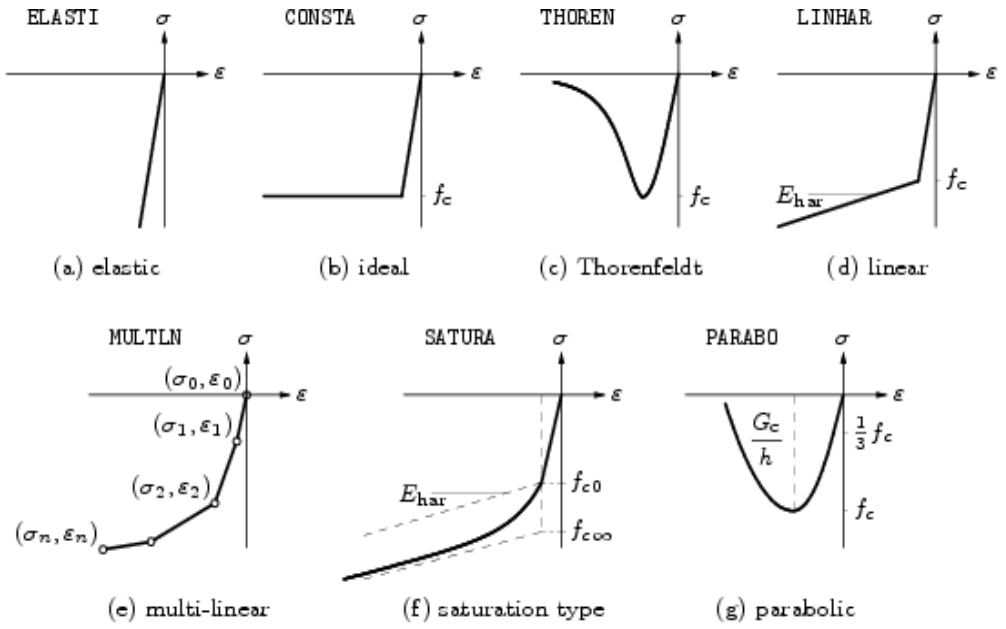

Figure 2.9 Compressive behavior for total strain crack model, from (TNO Diana, 2009).

2.3.4 Finite element analyses of slabs

Many researchers have analyzed corner-supported two-way slabs with square shape in plan. The slab is subjected to concentrated load in the middle of the span; the ratios of the reinforcement in both directions are equal and only one quarter of the slab is modeled due to the symmetry, see Figure 2.10 .

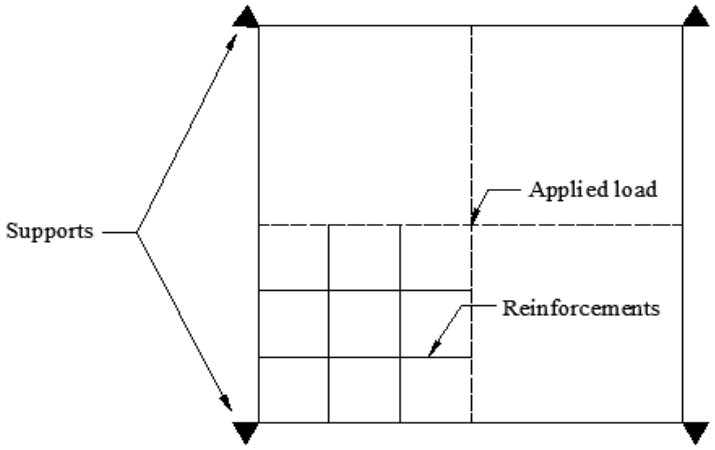

Figure 2.10 Slab studied slab many researchers, from (Hyo-Gyoung, Filip Filppou, 1990).

The researchers used load-deflection diagrams to compare the experimental data with proposed tension-stiffening models which are based on fracture energy. The observation of a few researchers will be discussed in the following.

McNeice (1971) used effective stiffness approach. Both steel and concrete were considered as elastic materials. Lin and Scordelis (1975) considered steel and concrete with elasto-plastic behavior and coupling effect between membrane and bending action in the slab were taken into account. Hand, Pecknold and Schnobrich (1973) researched in-plane deformation and shear without considering the tension stiffening effect. By comparing experimental results with analytical and finite element outcomes, the following conclusions were drawn: Tension stiffening has a prominent effect in analysis of slabs; it is more important in RC slabs than beams. Hyo-Gyoung, Filip Filppou (1990), figured out that tension-stiffening increases the stiffness of the member since tensile stress between cracks are included in the analysis.

In 2013, Blanco modeled real scale SFRC two-way slabs with different widths using the FEM software ATENA. Four rectangular and two squared shape slabs were tested and all the slabs were simply supported in the center of each edge line, see Figure 2.11.

Figure 2.11 Test specimen, from (Blanco, 2013)

Displacement control was used to compare the results. The concrete tensile behavior was modeled from the combination of non-linear fracture mechanisms with smeared crack approach and crack band method. The results showed that:

- Four main crack patterns in the slabs occurred which were initiated from the center of the slabs to the edges where supports were located; see Figure 2.12(a). In case of slabs with larger dimensions, secondary cracks appeared due to larger deformations; see Figure 2.12(b).
- Different distribution of the fibers in the concrete mix had a large influence on the crack patterns.

a) **b)**

Figure 2.12 Crack pattern, from (Blanco, 2013)

3 Modeled experiments

3.1 Description of the modeled experiments

3.1.1 Dimensions

The tests modeled in this thesis were carried out at Chalmers University of Technology; see (Fall, Rempling, & Lundgren, 2013). Nine octagonal concrete slabs have been tested: Three with conventional reinforcement, three with only fiber reinforcement and one with combined reinforcement. In this thesis, one representative test of each type was used for comparison to analysis the results. The specimens were subjected to a concentrated load in the middle of the slab. A steel plate was placed in the center of the slab to distribute the concentrated force, see Figure 3.1.

Dimensions of the slab are shown in Figure 3.2.

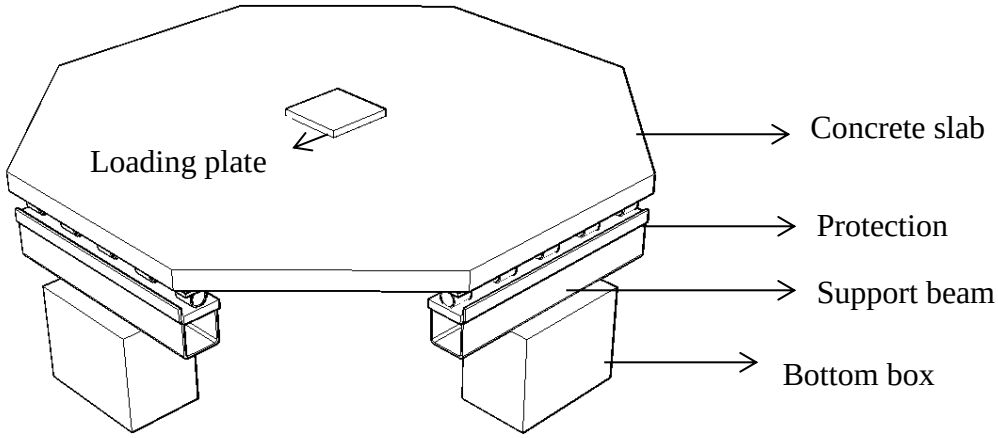

Figure 3.1 Test set-up

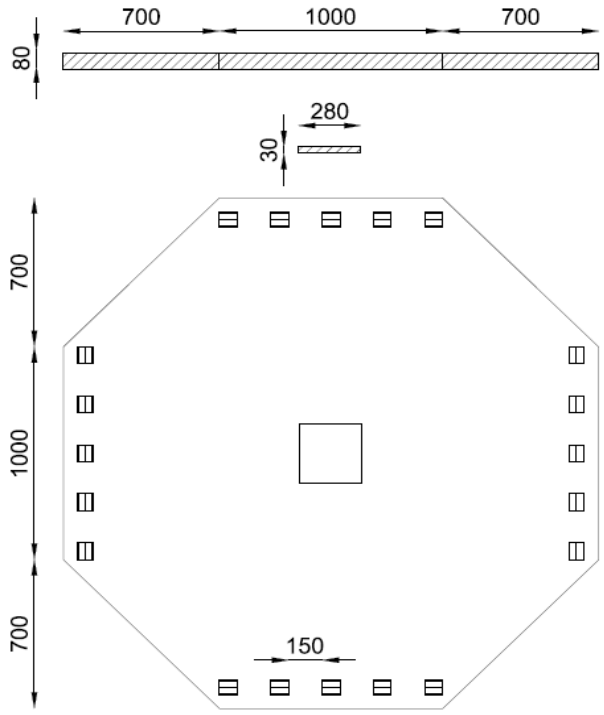

Figure 3.2 Dimension of one slab [mm]

3.1.2 Support

The slabs were simply supported on four edges where each side consisted of five roller supports (see Figure 3.1). Two steel plates were located on top of rollers which were adjustable by bolts, which made it possible to change the height of the steel plate. As a safety measure, barriers were inserted to prevent the rollers from sliding out too far, see Figure 3.3. The rollers were never in contact with these barriers during the tests.

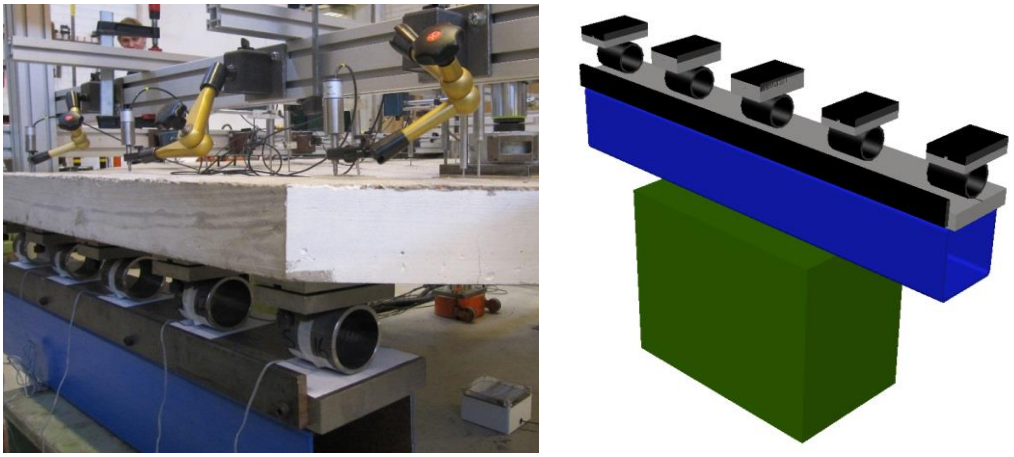

Figure 3.3 Support

3.1.3 Reinforcement

The steel bars used in this experiment had a diameter of six millimeter ($Ø_s$=6mm); in the different directions they were arranged on top of each other (like a grid). In the strong direction (*y*-direction), 25 bars with spacing of 98mm and in weak direction (*x*-direction), 13 bars with spacing of 196mm had been arranged, see Figure 3.4.

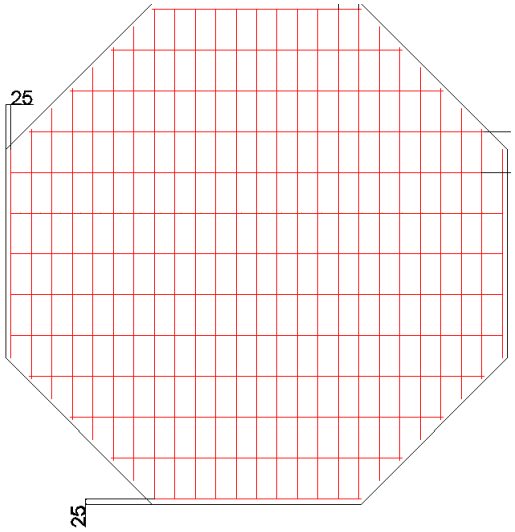

Figure 3.4 Reinforcement layout

3.1.4 Loading

The concentrated load was created by a hydraulic jack, which was applied in the middle of the slab. LVDTs (Linear variable differential transformers) were situated on top of the slab to measure the displacements in different points during the test, see Figure 3.5. The outer ones monitored the support settlements.

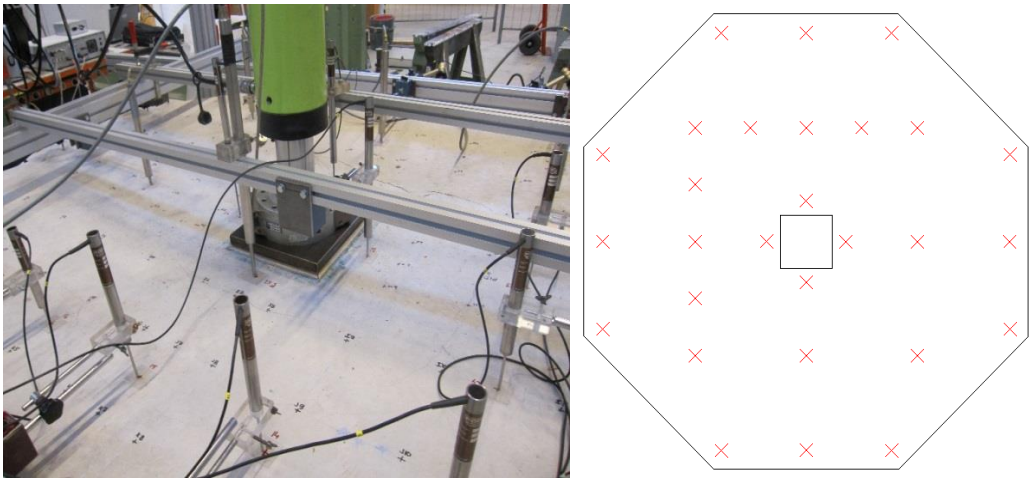

Figure 3.5 Location of LVDTs on one slab

3.2 Material tests

3.2.1 Concrete

For concrete in tension values were taken from uniaxial tensile tests, see (Rempling, Fall, & Lundgren, 2013). The measured mean tensile strength (f_{ct}) for plain and fiber reinforced concrete was 2.7MPa and 3MPa respectively. One of the important results, which should be emphasized, was the large difference in post cracking behavior of plain and fiber reinforced concrete. In plain concrete, after cracking there was almost no capacity left to carry the load; thus by increasing deformation, the load decreases to zero (brittle behavior), while fiber reinforced concrete can resist the load for much larger deformations; the fibers thus improve the ductility of the concrete, see Figure 3.6.

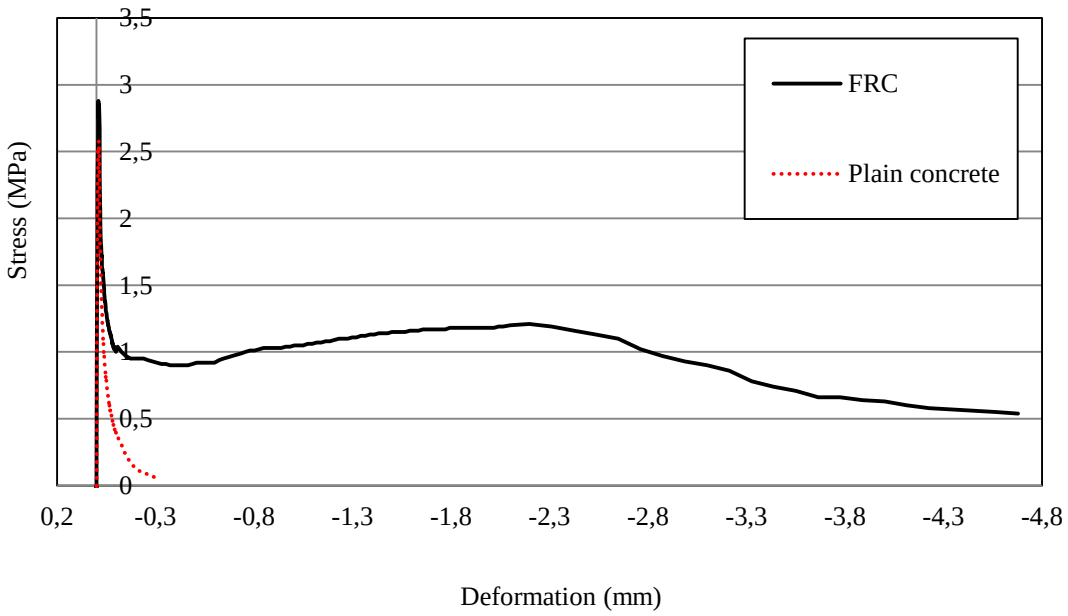

Figure 3.6 Tensile response for plain and fiber reinforced concrete, from (Rempling, Fall, & Lundgren, 2013)

3.2.2 Conventional Reinforcement

The conventional reinforcement used in the slabs had a modulus of elasticity of 210GPa and yield stress of 671MPa. The values were obtained from tensile tests and the stress versus strain diagram based on nominal bar area is shown in Figure 3.7.

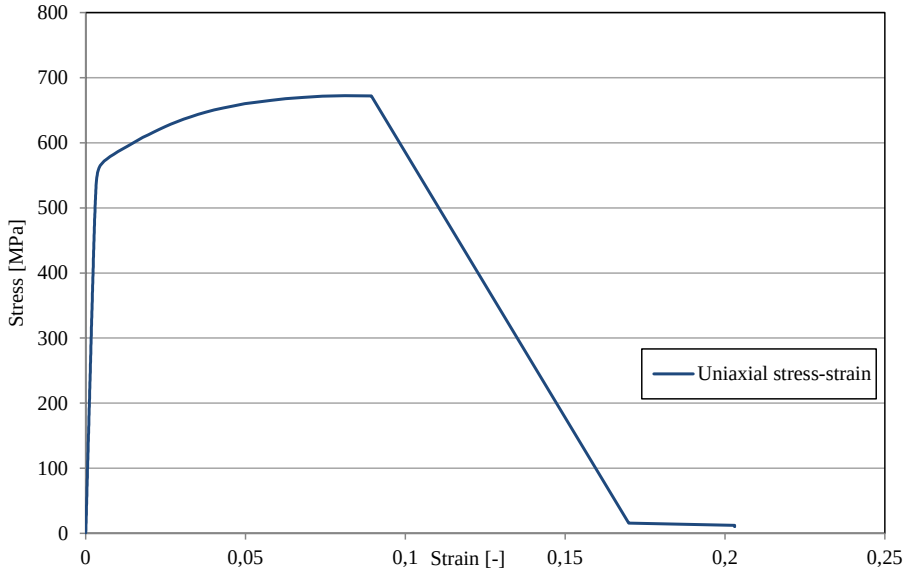

Figure 3.7 Uniaxial stress-strain diagram

3.2.3 Steel Fiber Reinforcement

The steel fiber used in this experiment is called Dramix® 5D with a length of 60 mm and diameter of 0.9 mm (Figure 3.8). These fibers are shaped to form an anchor, keeping the fiber firmly in place inside the concrete. Under tension, the wire is elongated, providing ductility on the same principle as traditional reinforcement steel (Bekaert). The material properties are shown in Table 3.1.

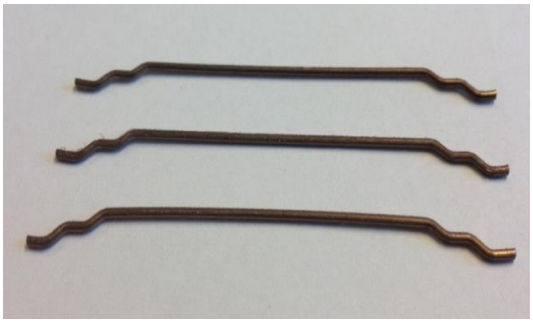

Figure 3.8 Dramix® 5D

Table 3.1 Properties of Dramix® 5D

l_f (mm)	$Ø_f$ (mm)	f_{ft} (MPa)	E_{sf} (MPa)
60	0.9	2300	210

3.3 Summary of experimental data

The data for different studied slabs is shown in Table 3.2. The data was provided by experimental tests in Chalmers University of Technology.

Table 3.2 Experimental data

	Conventionally reinforced slab	**Fiber reinforced slab**	**Fiber+ Conventional reinforcement slab**
f_{ck} [MPa] (cylindrical specimen)	51.18	44.70	44.70
f_{ct} [MPa]	2.7	3.0	3.0
E_c [GPa]	31.7	31	31.0
ρ_c [kg/m^3]	2312	2327	2327
h [mm]	84	79	82
f_y [MPa]	560	-	560
f_u [MPa]	672	-	672
E_s [GPa]	210	-	210
ρ_s [kg/m^3]	7500	-	7500

4 Finite element analysis

As mentioned earlier, 2D curved shell elements were used as the element type and slabs with different reinforcement (conventional, fiber and combination of both) were studied to understand their structural behavior in different stages, i.e. at cracking, yielding and failure. Displacement control was used, and the load versus deformation, load distribution and crack pattern for each type of slab was compared with the experimental results. Another part of this thesis was to investigate the effect of different parameters and observe their influence on the structural level. These variations were applied on the analyses of slabs with only conventional reinforcement.

4.1 Geometry and boundary conditions

Due to the symmetry and to save computational time, only one quarter of the slab was modeled. The loading plate was modeled on top of the slab using rectangular elements with mesh size of 35mm. In order to have the same displacement in both of the loading plate and the concrete slab, tyings were used at the nodes between the concrete and the steel plate in the *x* and *y* direction, see Figure 4.1.

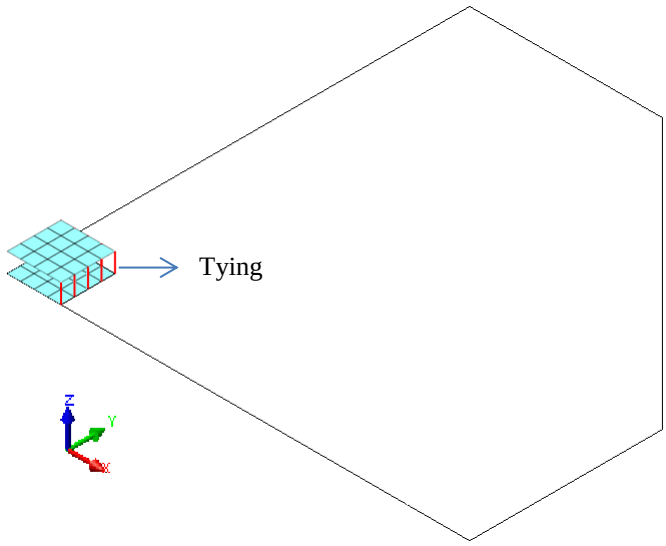

Figure 4.1 Geometry of the slab

Boundary conditions were defined as follows (see Figure 4.2):

- Symmetry boundary condition: These constraints were set along the symmetry lines on the symmetric part of the slab along *x* and *y*-axis.
- Simply supported boundary conditions: In the nodes where the roller supports were located in the experiments, supports in the *z*-direction were applied.

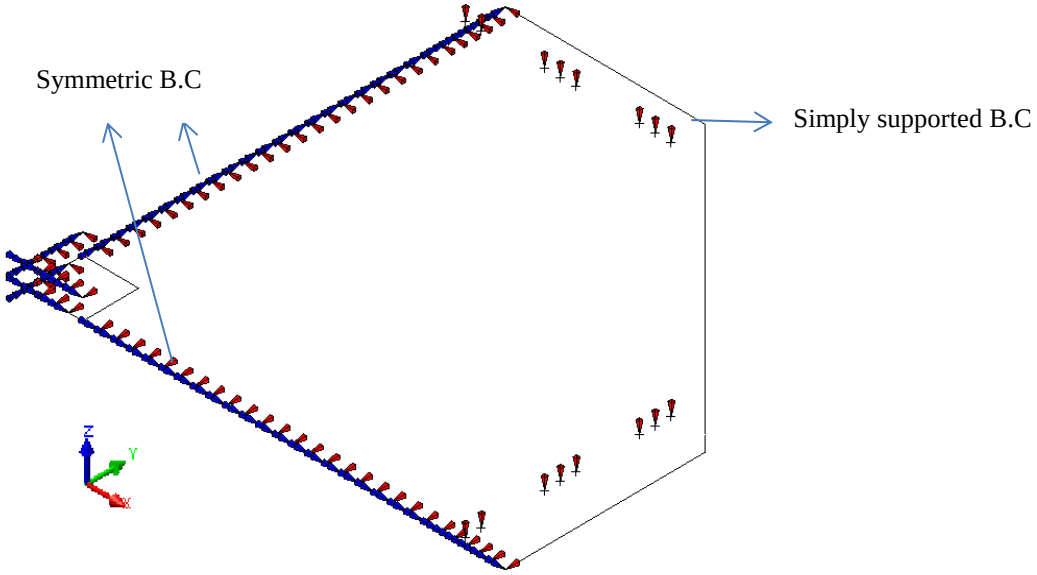

Figure 4.2 Boundary conditions

4.2 Reinforcement

Twelve bars were placed in the strong direction (*y*-direction) and six in the weak direction (*x*-direction), see Figure 4.3. The spacing between the bars was the same as in the tests. Complete interaction between concrete and reinforcement was assumed, thus embedded reinforcement was used to model the reinforcement.

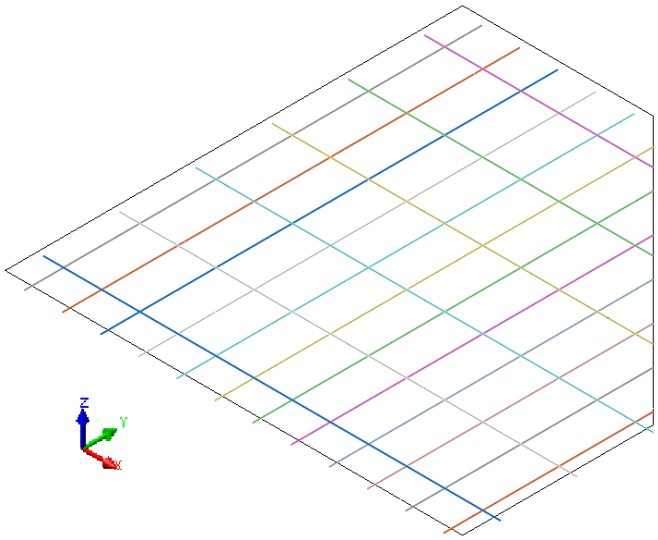

Figure 4.3 Reinforcement arrangement

Von Mises plasticity model was used for the reinforcement and to specify the hardening, translation of uniaxial experimental data had to be done to equivalent plastic strain, with initial yield stress of 555 MPa, see Figure 4.4.

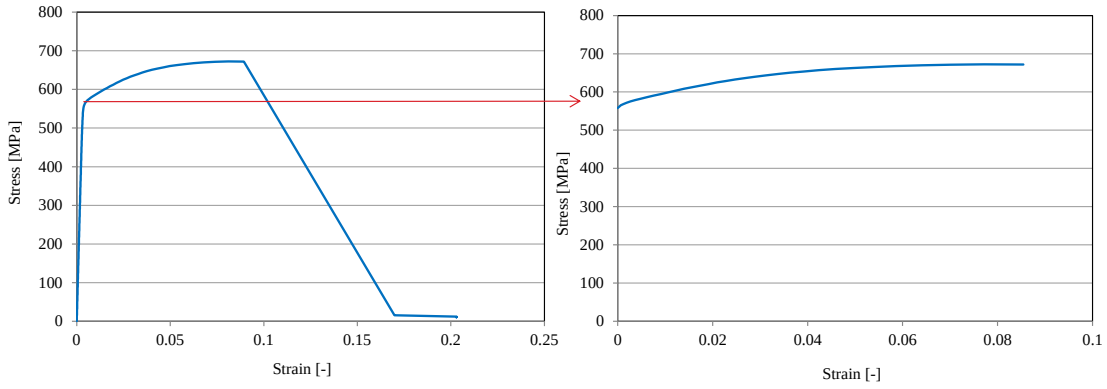

a) Uniaxial stress-strain **b) Equivalent strain-hardening diagram**

Figure 4.4 Derivation of hardening diagram for reinforcement.

4.3 Reference case

Conventional reinforced concrete slabs were chosen as the reference case in this study and all of the varying parameters in the rest of the work were compared to this model, see Figure 4.5. In the concrete part of the slab, CT30S elements were used which implies triangular elements with mid-side nodes and for the steel plate, quadrilateral elements with mid-side nodes (CQ40S) were adopted. In both of the element types, integration scheme over the thickness was Simpson and over the area, Gauss was used. The element size for both triangular and quadrilateral elements was 35mm, which was also the chosen crack band width. Details regarding element types, mesh alignment and integration points are discussed in chapters 4.5.1, 0 and 0 respectively. Poisson's ratio of 0.15 and 0.3 were chosen for the concrete and reinforcement correspondingly, and other material properties are shown in Table 3.2. A displacement was defined as the applied load in the center of the steel plate and tyings were used to spread the load to other nodes in the steel plate as well. More details regarding different alternatives for applying the load is discussed in chapter 0. To model the supports, interface elements were used to allow uplifting, refer chapter 4.4. Multi-linear tensile curve was used to specify the tensile behavior of the concrete, see chapter 4.10.

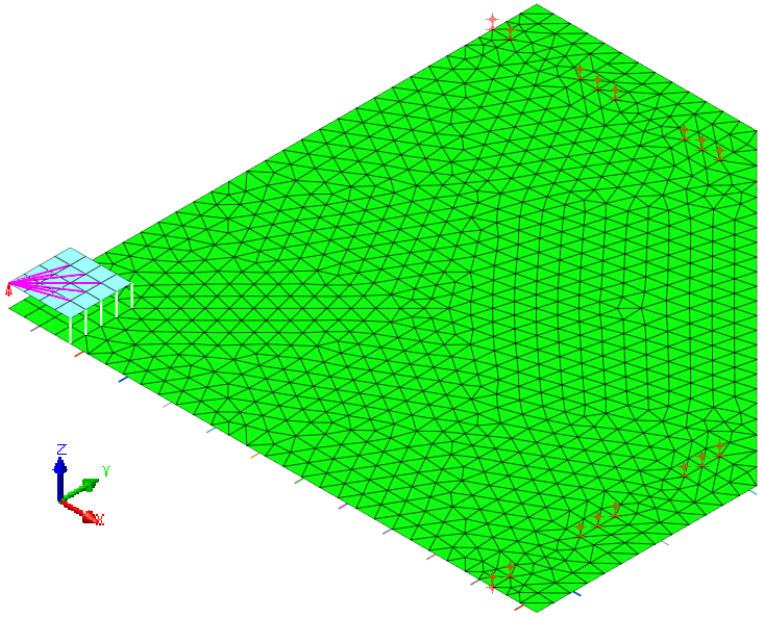

Figure 4.5 Reference slab model

Steel bars were used as reinforcement in both directions and embedded reinforcement concepts were used. Detail and arrangement of the reinforcement are described in chapters 3.1.3, 0 and 0. Yielding of the reinforcement was observed from their related stress diagrams in post-processing analysis. According to load-deflection diagram in Figure 4.6, step a, shows the initial yielding of the reinforcement which was started in the strong direction (*y*-direction). Step b indicates yielding of the reinforcement in both directions and it continued until they could not carry any more load and failure happened (step c).

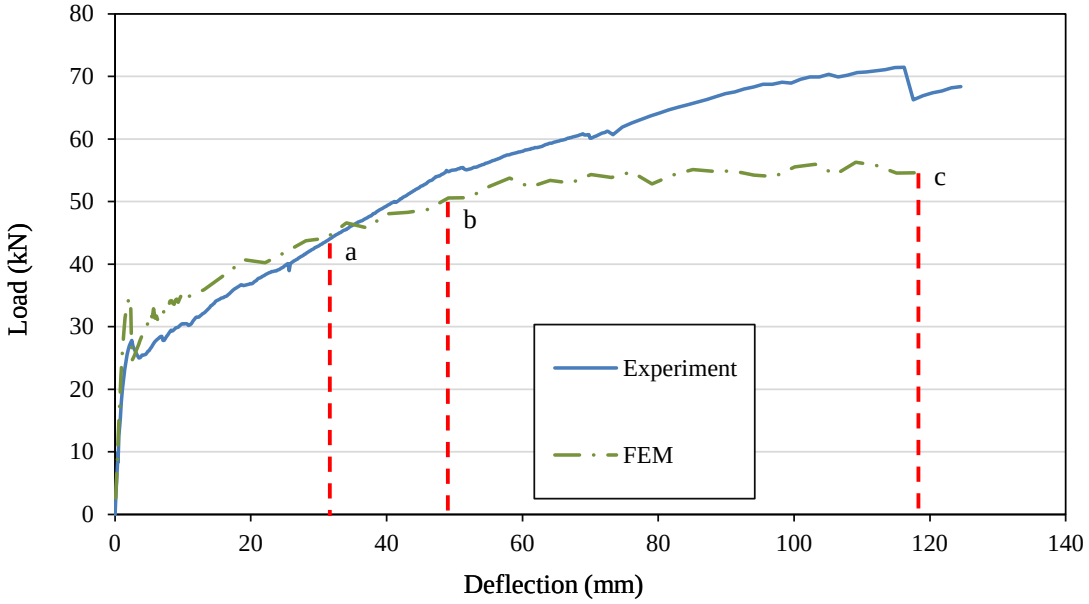

Figure 4.6 Load- deflection diagram for steps a, b, and c

Contour plots for the reinforcement in all of the chosen steps are shown in Figure 4.7

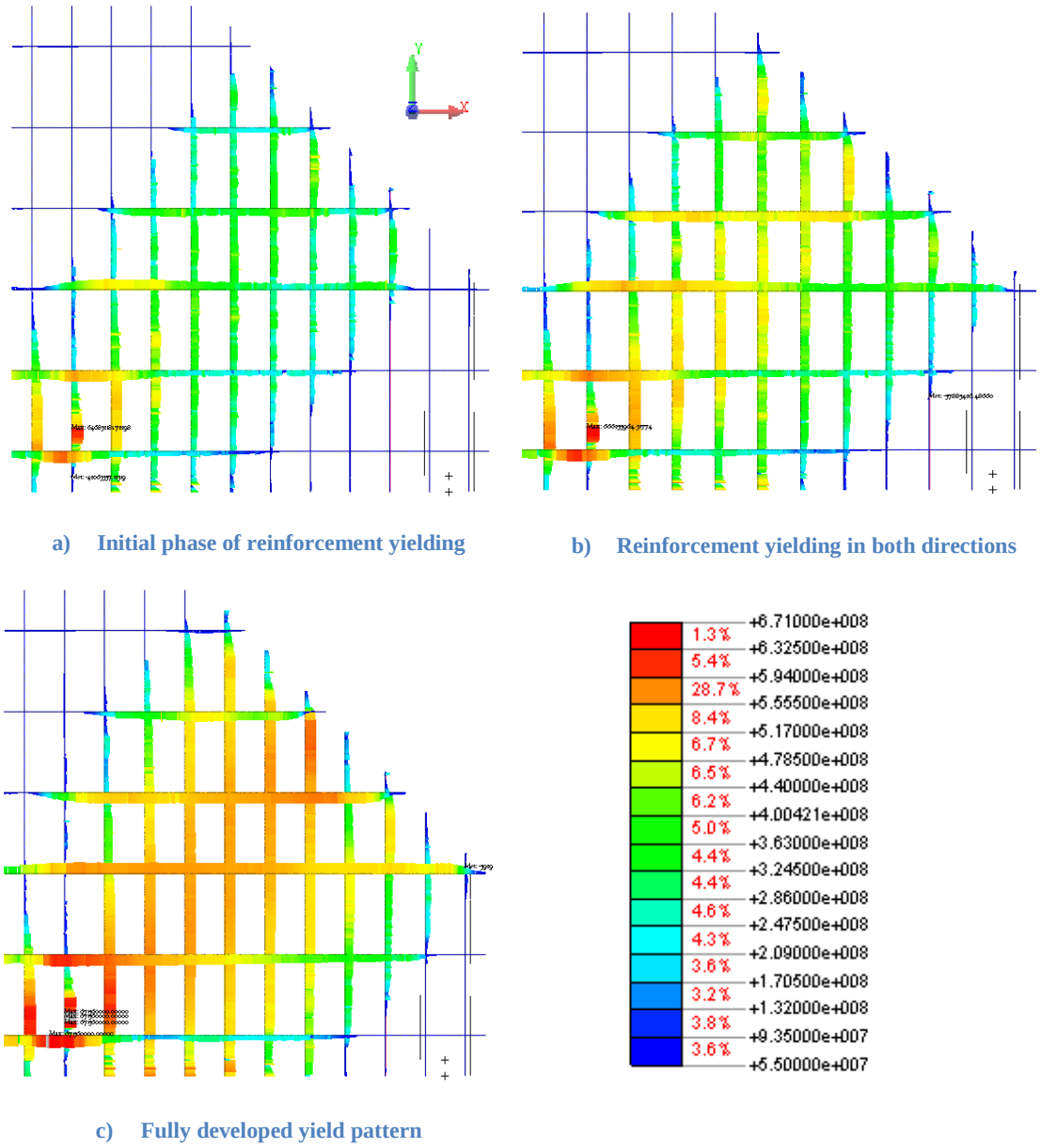

a) Initial phase of reinforcement yielding

b) Reinforcement yielding in both directions

c) Fully developed yield pattern

Figure 4.7 Yielding of the reinforcement in reference model

The results of the reference model are compared to experimental in Figure 4.*8*. On the cracking point (Figure 4.*8*, point A), the FE analysis has a slightly higher capacity compared to the reality and this remains until the reinforcement started to yield in the analyses, see Figure 4.*8*, point B. From that point until failure (point C), slightly lower stiffness and lower ultimate load was obtained in the analysis compared to the experiments.

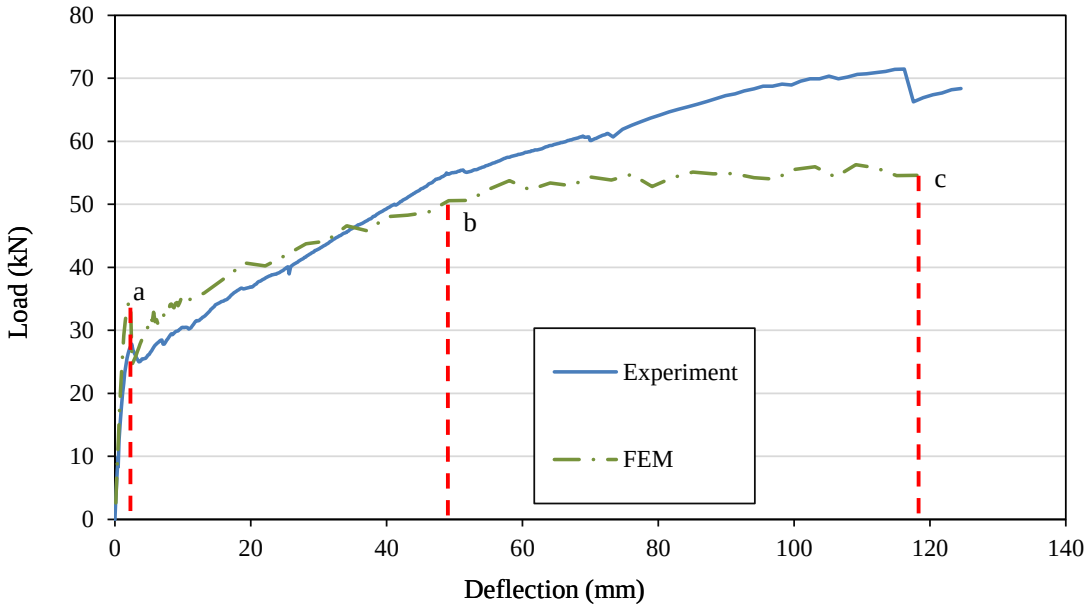

Figure 4.8 Load-deflection results for reference model (conventional reinforced slab)

The cracks were plotted in three different steps on the load- deflection diagram with a fixed strain range between 0 and 10^{-3}, see Figure 4.9.

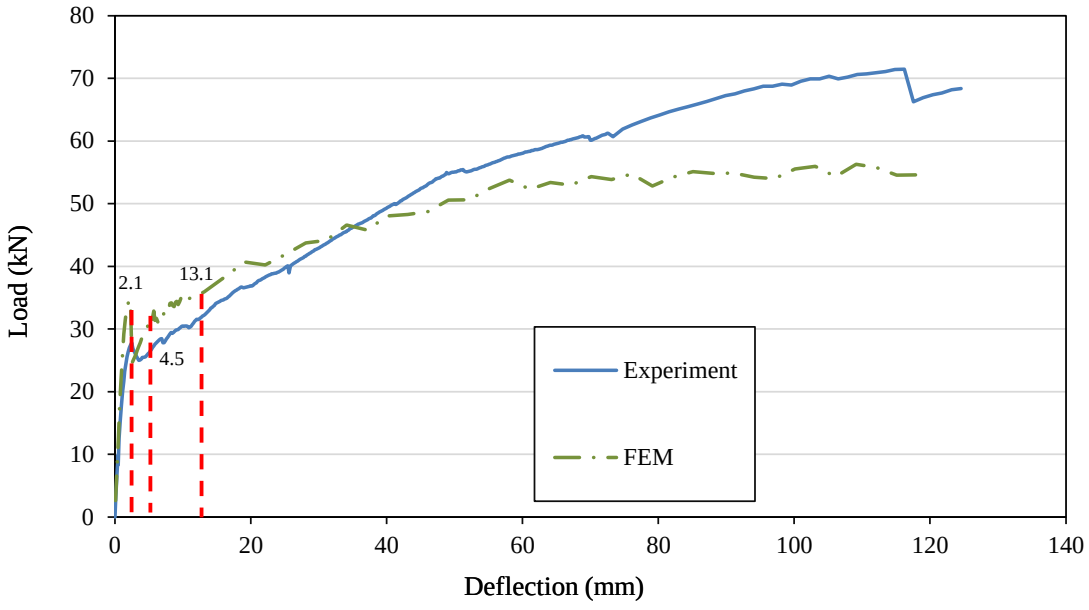

Figure 4.9 Different chosen steps for plotted cracked patterns

Crack pattern and development in the experiment and reference analysis are shown in Figure 4.10 and Figure 4.11 respectively. The initial crack occurred in the middle of the slab, under the steel plate, where the stress reached maximum tensile strength (Figure 4.10a). By increasing the load, several small cracks evolved until unifying into one continuous crack (Figure 4.10b). Figure 4.10c shows when the cracks were smeared over the region.

Comparing the crack patterns from FEM and experiment revealed that very similar results were obtained; the first crack appeared in the most stressed region, and later several cracks were formed from the middle to the free edges of the slab (where there was no support).

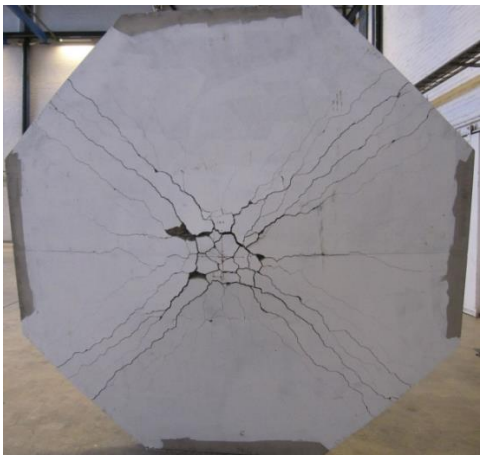

Figure 4.10 Crack pattern from experiment

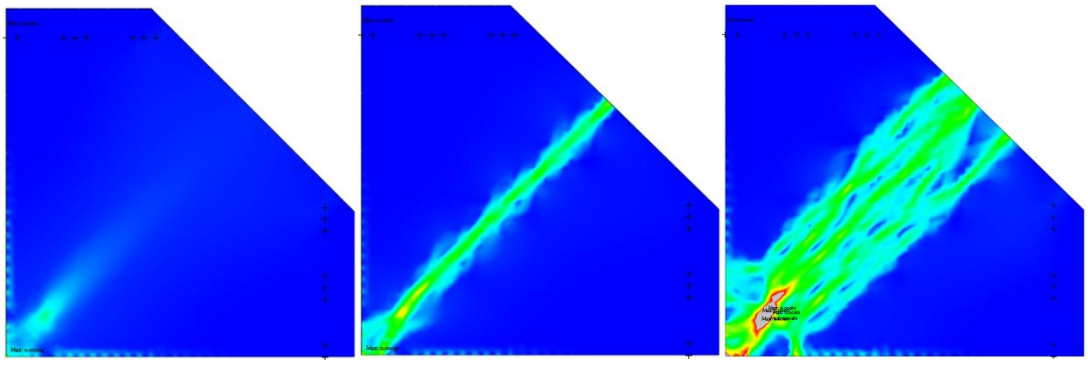

a) 2.1mm **b) 4.5mm** **c) 13.1mm**

Figure 4.11 Crack pattern for the reference model in FE analysis for related deflection

4.4 Modeling of the supports

Three nodes were defined as supports for each roller in the model and all of the nodes were supported in the vertical direction (*z* direction, simply supported). Two different modeling approaches of the supports were investigated in this section:

In the first model, the supports were set on the nodes without considering interface elements (preventing uplift); see Figure 4.12 (a).

In order to allow uplifting, non-linear elastic interface elements were added between the supports and the slab, see Figure 4.12 (b). For the interface elements, a multi-linear function, with a very high stiffness value in compression ($2.1*10^{12}$ N/m) and low in tension (1 N/m) was defined.

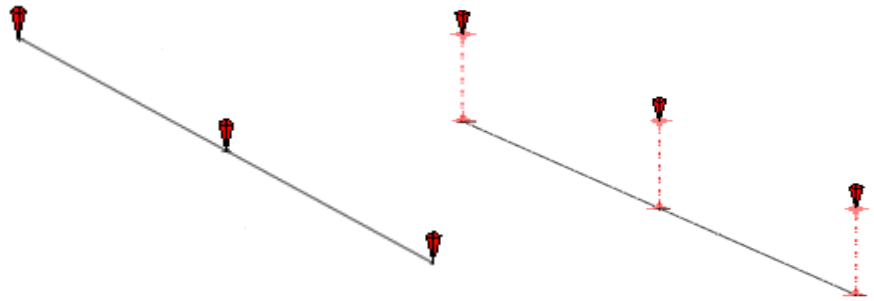

a) Supports without interface elements **b) Using interface elements**

Figure 4.12 Support modeling

Load-deflection diagram for both fixed and allowing uplift analysis were drawn and the results were quite similar. To try to solve this, another analysis was conducted where three times lower stiffness was assigned for the interface elements but it did not affect the results that much, see Figure 4.13.

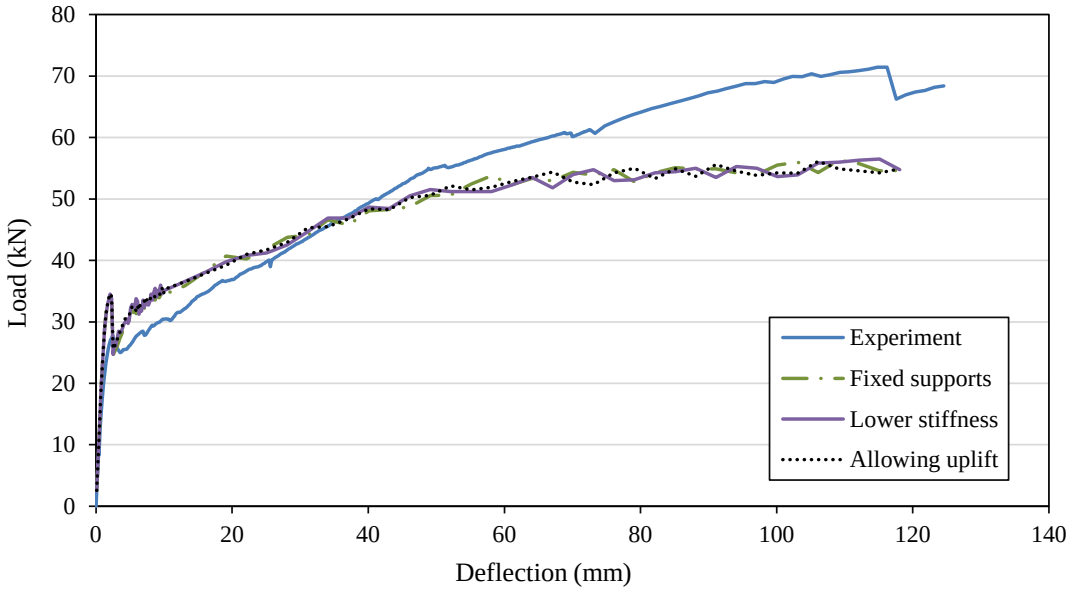

Figure 4.13 Load-deflection results for different support modeling alternatives

Figure 4.14 shows the applied load versus reaction forces when the uplift is allowed and prevented and better results were reached when uplifting was allowed in the supports.

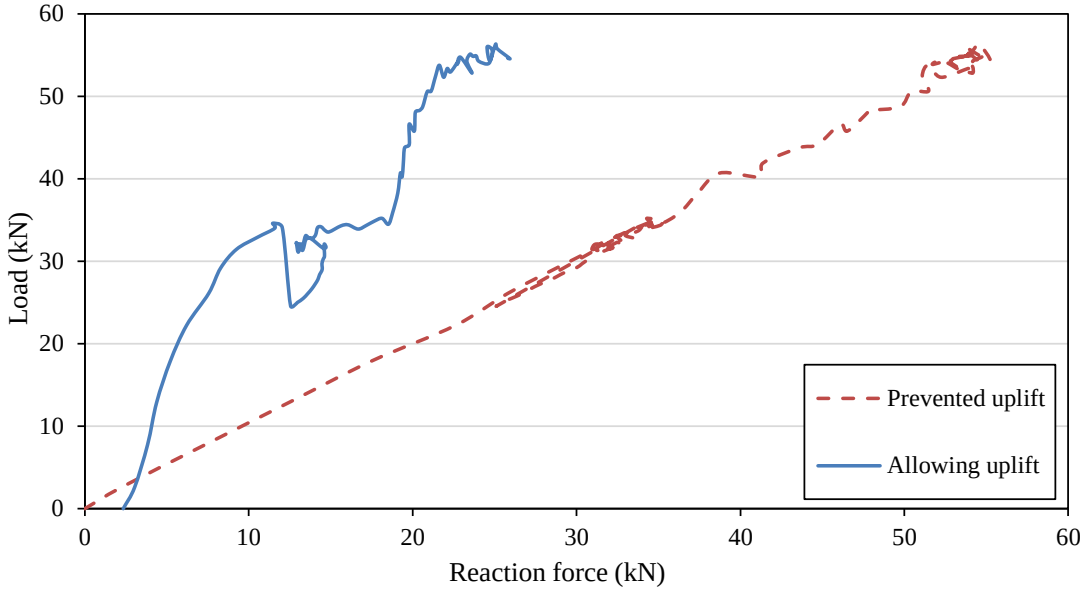

Figure 4.14 Applied load versus reaction force

The distributions of the support reactions were investigated and the results were presented in this section. Geometry and location of each support were explained in chapter 3.1.2 and, due to symmetry, only half of the supports were modeled in this study. Average values were used in strong and weak direction for supports (2&4) and (1&5) for the experimental results which were obtained from the laboratory tests, and in the FE model, the middle support (3) was multiplied by two and reaction forces for supports 4 and 5 were assumed the same as the reaction forces in supports 2 and 1, see Figure 4.15.

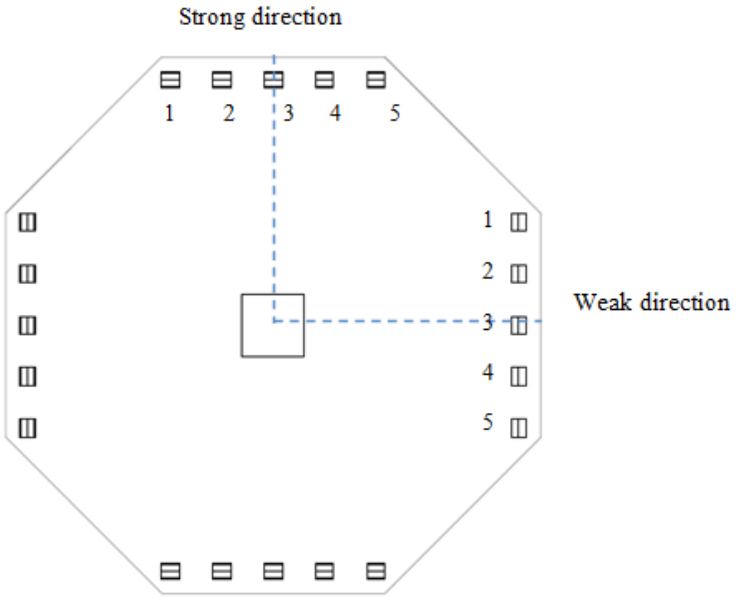

Figure 4.15 Studied support reactions

Three different steps were chosen in points before cracking (A), after cracking (B) and close to the reinforcement yielding (C); The results in both strong and weak direction were compared, see Figure 4.16.

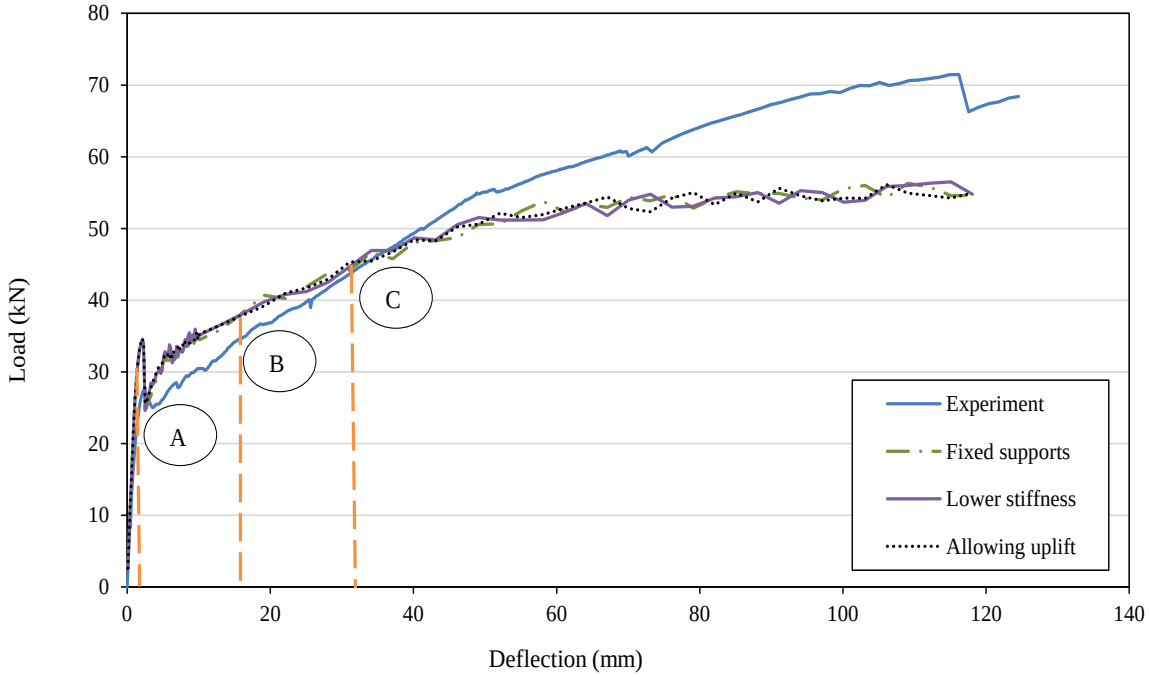

Figure 4.16 Chosen steps for studied reaction forces

Figure 4.17 and Figure 4.18 shows the related diagrams for each step (A, B and C) when the uplift was allowed and prevented in strong direction, respectively. The x-axis indicate the number of supports while the y-axis represent the proportion of the reaction forces in relation to the total applied load for each support in percentage.

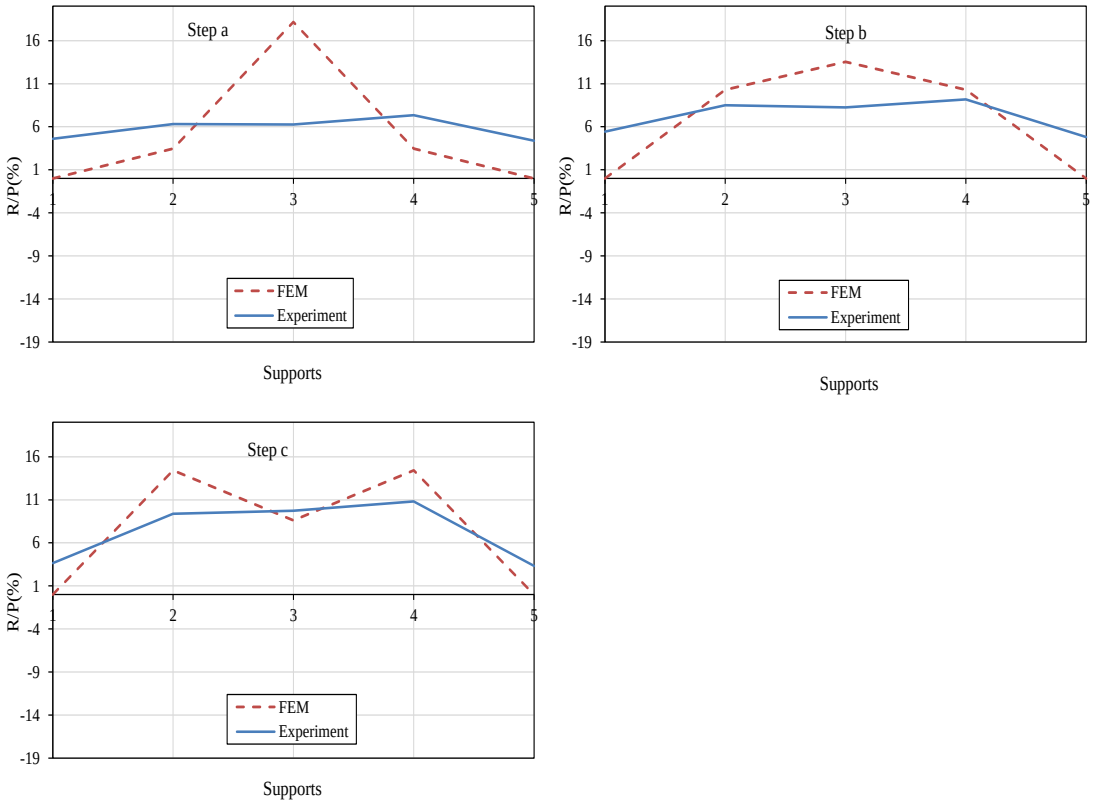

Figure 4.17 Support reaction in strong direction, allowing uplift

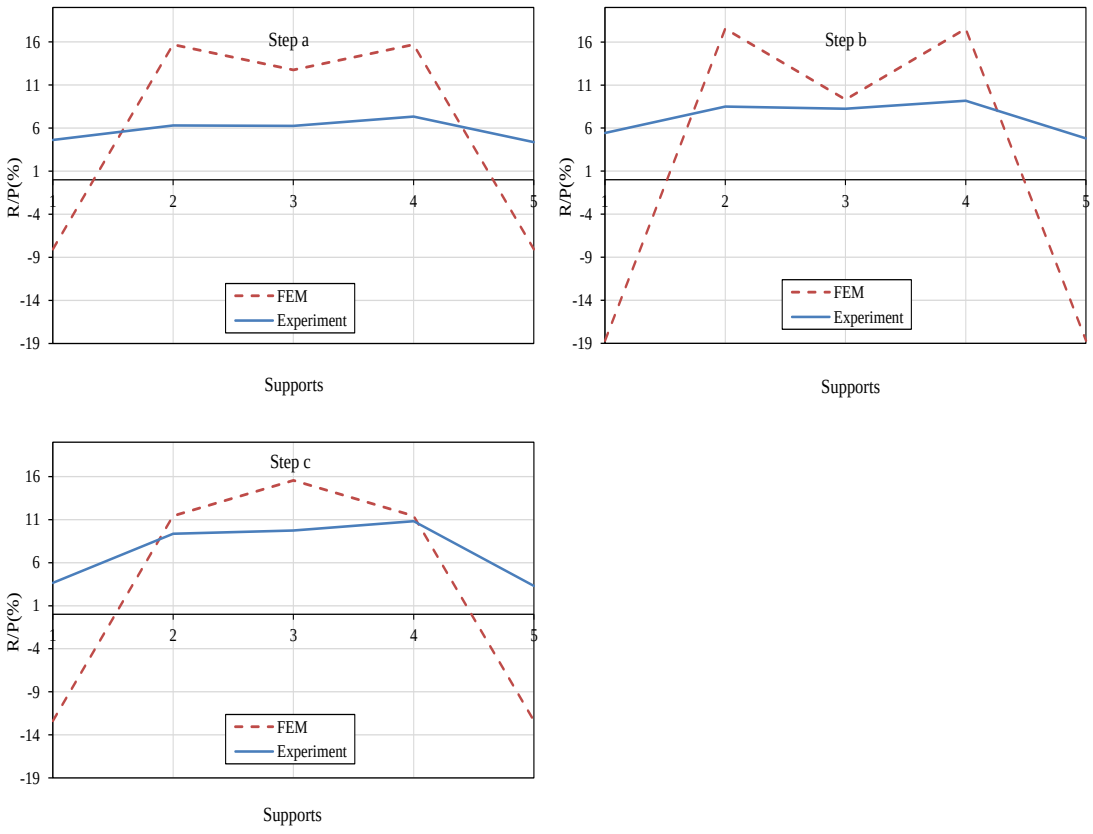

Figure 4.18 Support reaction in strong direction, preventing uplift

The results in the strong direction revealed an overestimation in FEM model in all of the steps for both cases compared to the experiment. The closest results were seen in the supports 2 and 4 (Figure 4.15) when uplift was allowed and the most deviating results from the analyses were seen at the same supports when uplift was prevented. In total when the uplift was allowed better results were obtained.

Figure 4.19 and Figure 4.20 shows how much load each support carried in the weak direction when uplift was allowed and prevented, respectively. The analysis results in this direction showed that in steps A, B and C, more accurate results were reached when the uplift was allowed.

By comparing the results in both strong and weak directions, it can be concluded that more load was resisted in the strong axis because of the larger reinforcement amount and also negative reactions were seen in the FE model at the edge supports when the uplifting was prevented.

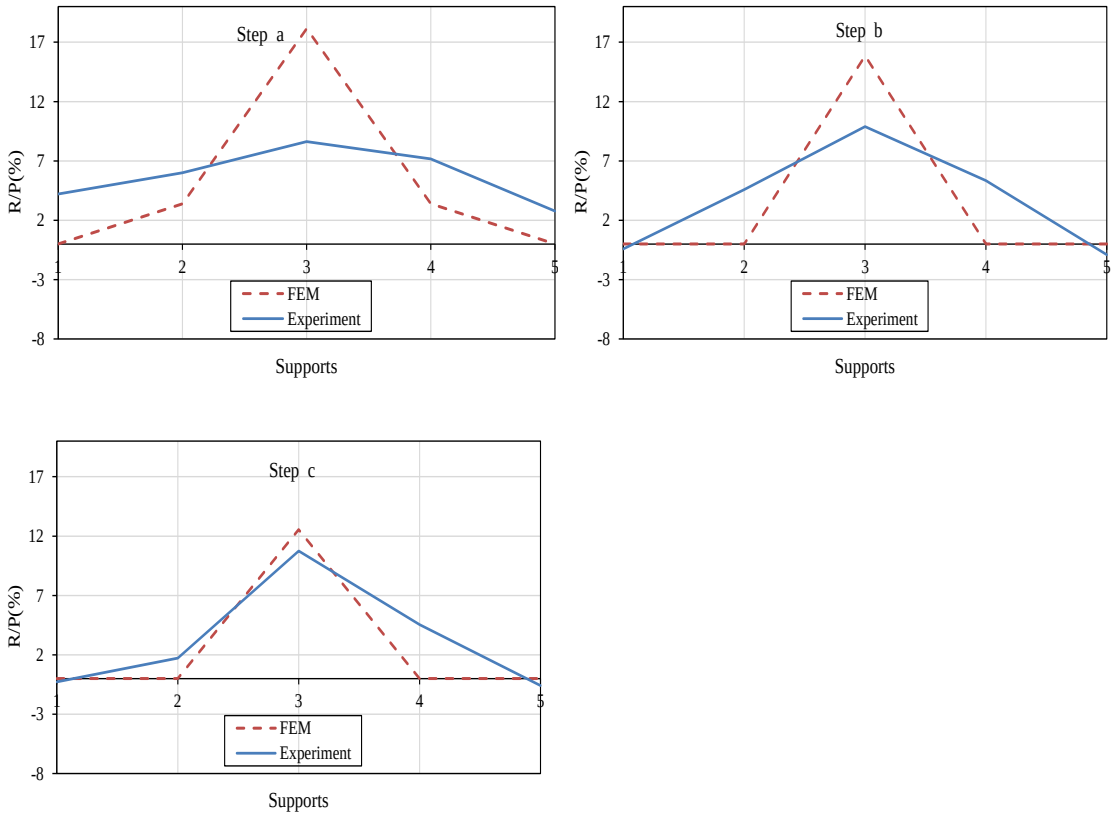

Figure 4.19 Support reaction in weak direction, allowing uplift

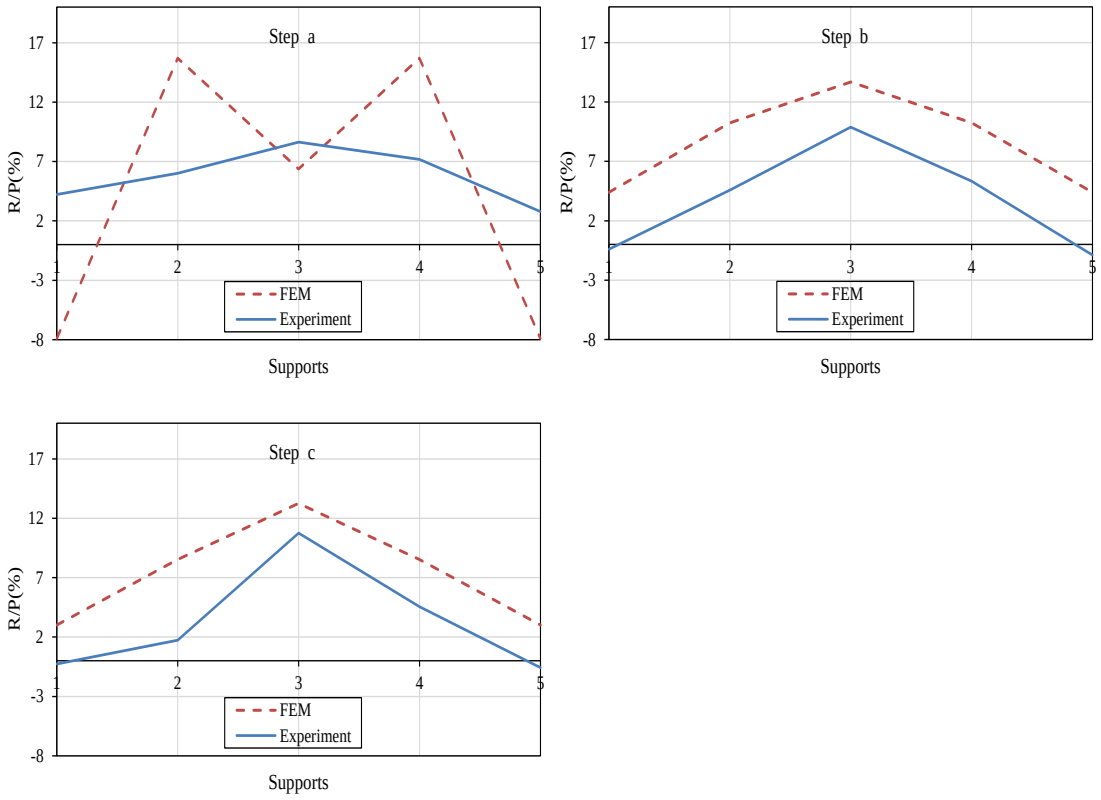

Figure 4.20 Support reaction in weak direction, preventing uplift

4.5 Mesh

To generate the mesh, dividing lines were used to create acceptable geometry regions. Automatic meshing was used to mesh the regions by selecting the relevant edges and its interior points (support nodes). The crack band width was assumed as same as the element size, which in the reference case was equal to 35 mm. For all of the elements, mid-side nodes were also generated. Some parameters such as element types, density and alignment of the mesh were examined for different cases in this case, which are explained on the following subchapters.

4.5.1 Mesh type

While the reference case was meshed with triangular elements, an alternative mesh with quadrilateral elements was also investigated. For the quadrilateral elements, CQ40S element was used which is an eight-node quadrilateral isoparametric curved shell element. These elements are based on quadratic interpolation and Gauss integration over the element area. For the triangular elements, six-node triangular isoparametric curved shell element CT30S was chosen, see Figure 4.21.

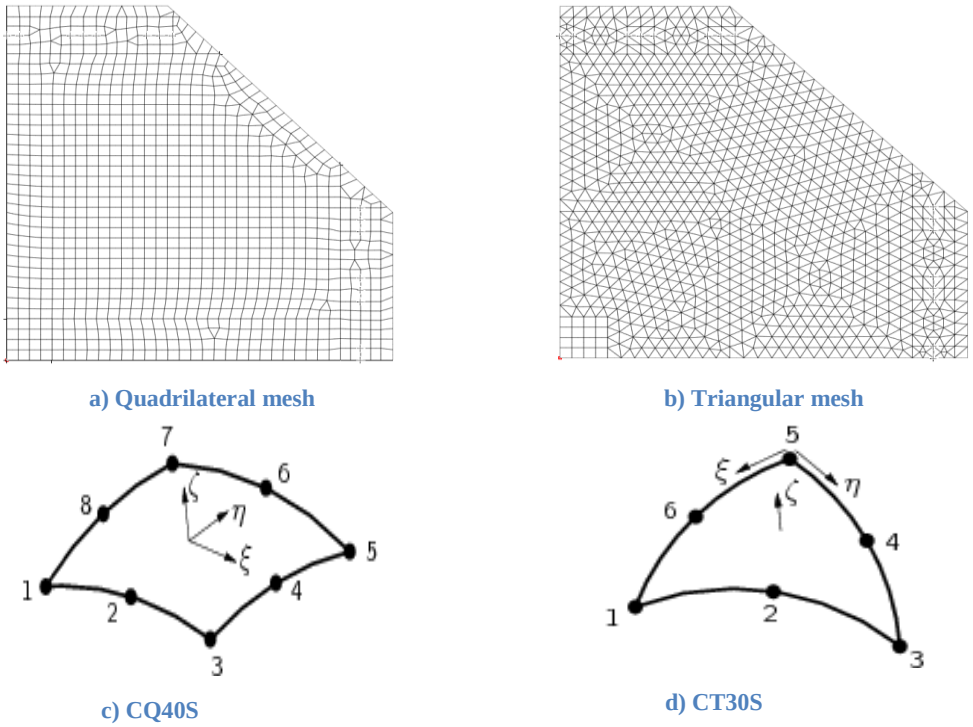

Figure 4.21 Different mesh and element types

The experimental and modeling results are shown in load-displacement diagrams in Figure 4.22. FE results for both quadrilateral and triangular meshes gave higher stiffness before cracking and underestimated behavior was seen in the post-cracking state, comparing to the experiment. The analysis results showed very minor differences; the analysis with triangular elements had slightly stiffer behavior compared to the analysis with quadrilateral elements. Furthermore, some problems were faced when meshing the slab with quadrilateral elements. It was not possible to mesh the whole models by using only quadrilateral elements; therefore a few triangular elements were also generated. This was time consuming because integration schemes had to be defined separately in .dat files for both triangular and quadrilateral elements.

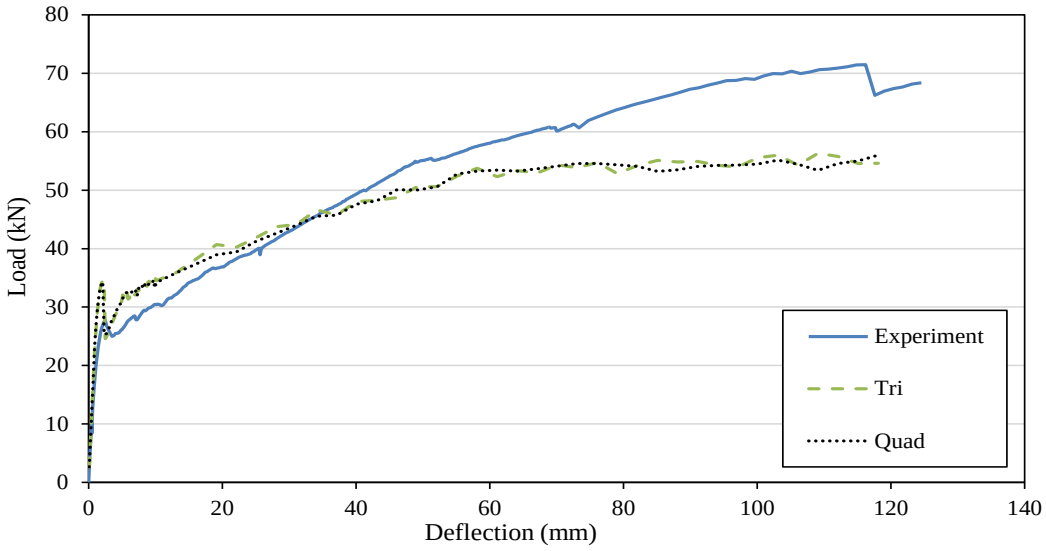

Figure 4.22 Load- deflection results for different mesh types

4.5.2 Mesh density

In order to investigate the effect of mesh densities, four different models with different mesh sizes were generated. All of the models were meshed by triangular elements. The reference model, which was used in the work, had a mesh size of 35 mm, see Figure 4.23a. Two models with finer meshes were created with half and a quarter mesh size of the reference model i.e. 17.5 and 8.75mm respectively, see Figure 4.23b and c. Another model with a coarser mesh was also generated, in which the mesh size was twice as large as in the reference model, i.e. 70mm, see Figure 4.23d.

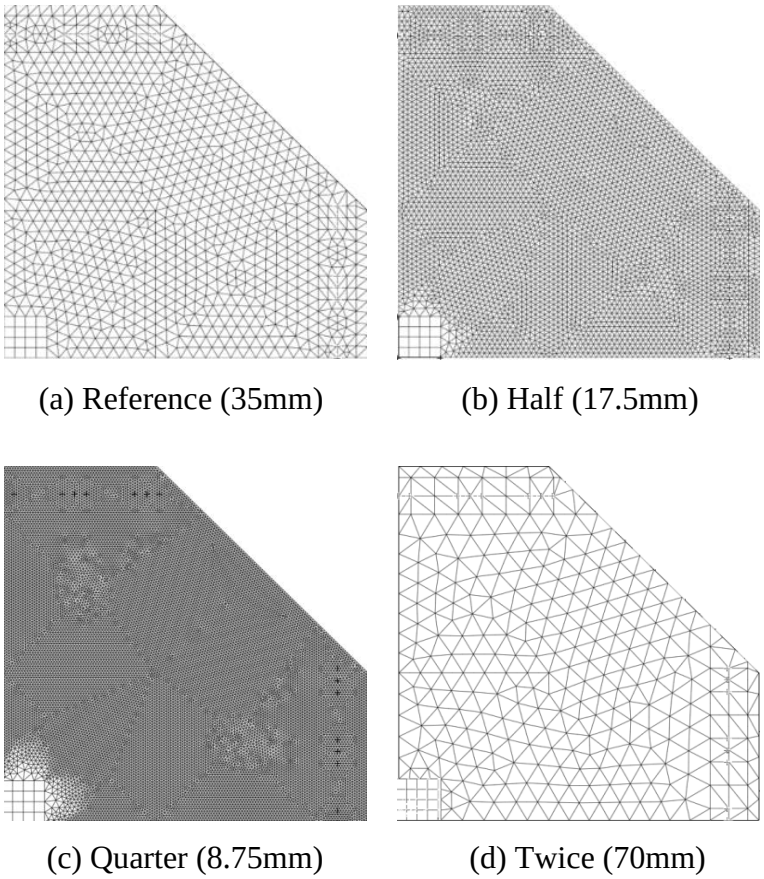

(a) Reference (35mm) (b) Half (17.5mm)

(c) Quarter (8.75mm) (d) Twice (70mm)

Figure 4.23 Slabs with different mesh densities

It is important to note that the crack band width was chosen to the element size in all these analyses. The results show that the models which were meshed with finer meshes, had higher cracking point and stiffer behavior while in the model with larger mesh size, lower cracking point and less stiff behavior was reached. The results of this study are shown in a load-deflection diagram in Figure 4.24.

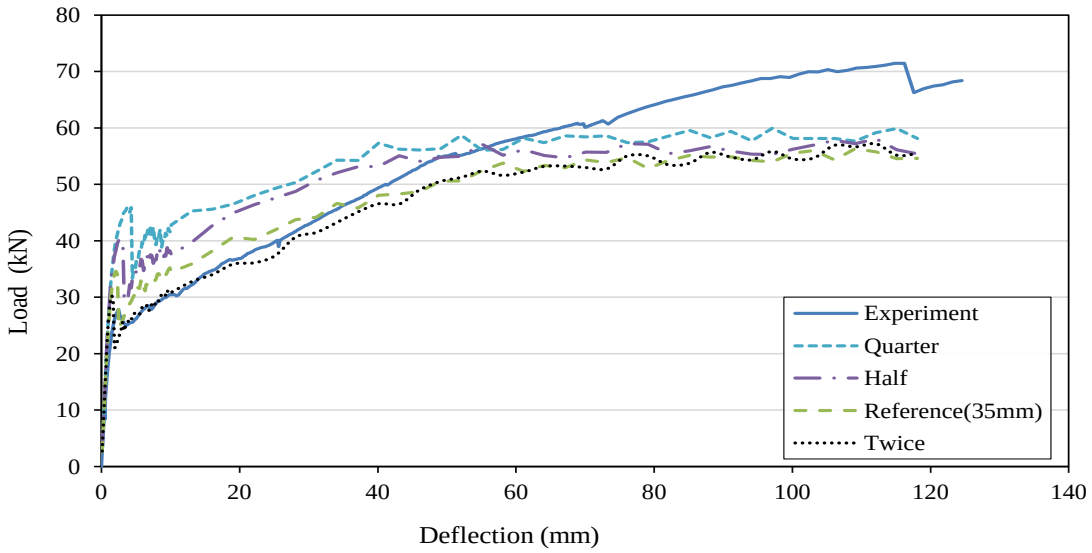

Figure 4.24 Load-deflection results for different choices of element size.

As the crack band width was chosen to be equal to the element size, this also varied in these analyses. In other analysis with different mesh densities a constant crack band width (35mm) was assumed. The results of these analyses are shown in Figure 4.*25*, as can be seen that the cracking point in all of the alternatives were the same, and the difference in the post cracking stage was small. As conclusion, when the crack band width was chosen as a constant value, changing the mesh densities, did not affect the results as much as when the crack band width was equal to the element size of each mesh.

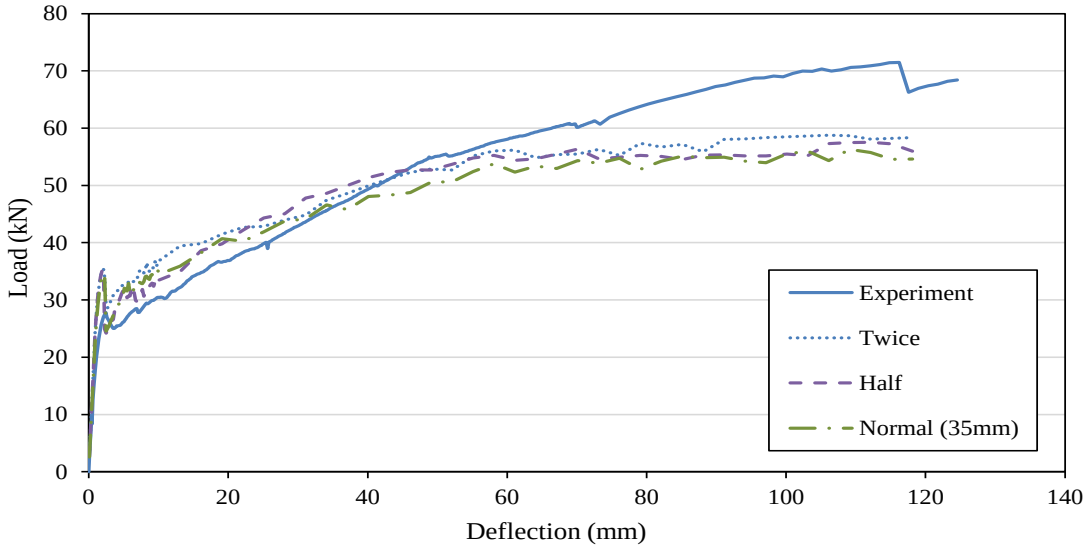

Figure 4.25 Load-deflection results for different choices of element size with a constant crack band width (35mm)

4.5.3 Mesh alignment

In order to study the effect of the mesh alignment two alternatives were considered. Figure 4.26 shows how these models were meshed; both of the models were meshed using triangular elements.

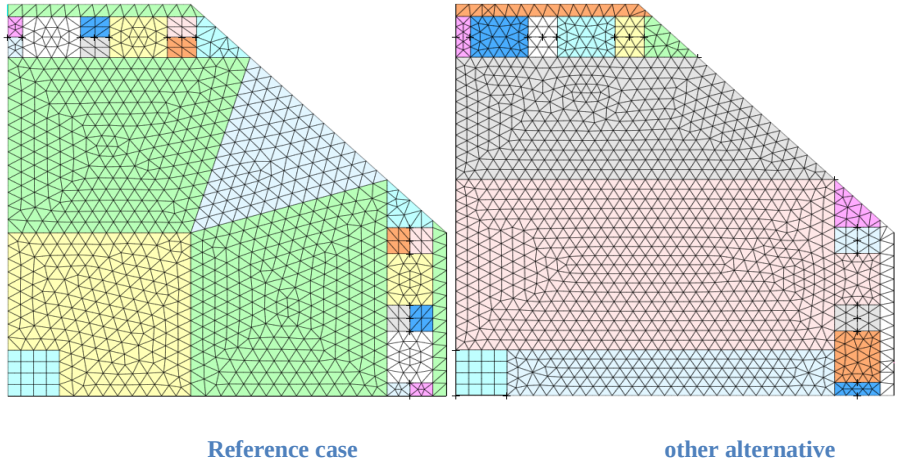

Figure 4.26 Different mesh alignments

The load-deflection diagram in Figure 4.27 shows that similar results were obtained in both of the models, but in some parts, the reference case showed slightly stiffer behavior compared to other alternative. Possibly it is so that the small differences are due to the use of triangular elements which give rather large freedoms for cracks to evolve in all directions; if the slabs were meshed by quadrilateral elements, mesh alignment might have led to more different results.

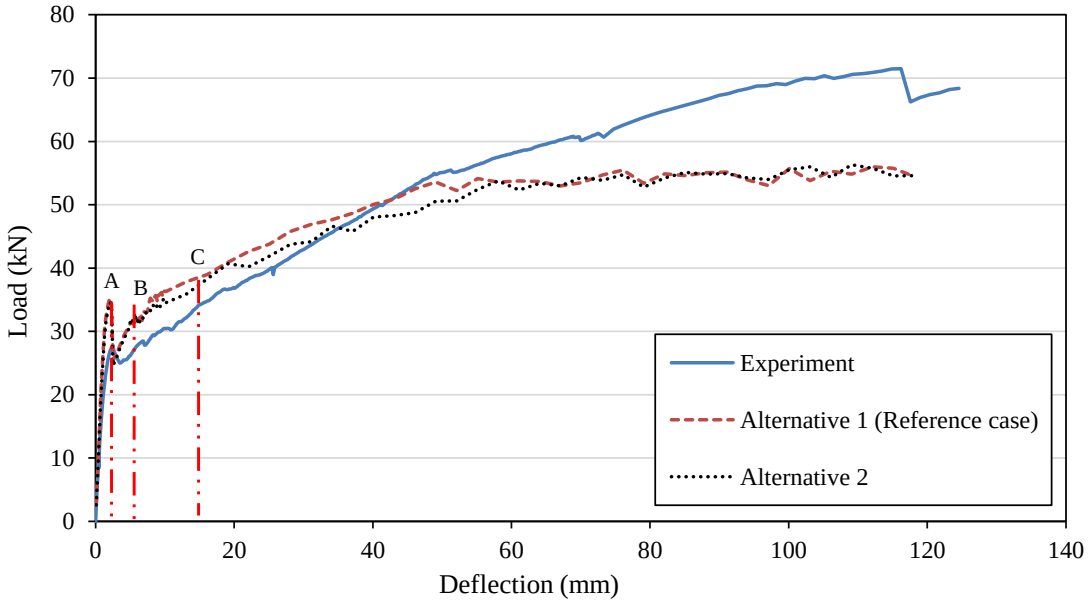

Figure 4.27 Load-deflection results for different mesh alignments

The crack patterns are from the same deflections, marked with A, B and C in Figure 4.27. Crack patterns for alternatives 1 and 2 are shown in Figure 4.28 and Figure 4.29 respectively. Comparing the crack patterns showed that in the reference case, propagation of the crack was like a thick line pattern with small fluctuation along it. On the other hand, by changing the mesh alignment, increasing the load resulted that, the crack propagation started to spread more to the adjacent areas and more fluctuation was seen in this case.

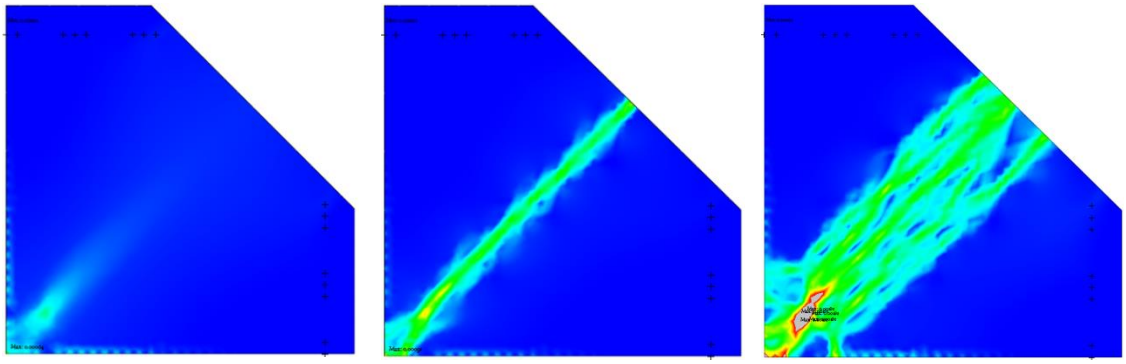

Stage A Stage B Stage C

Figure 4.28 crack patterns in reference model in different load steps

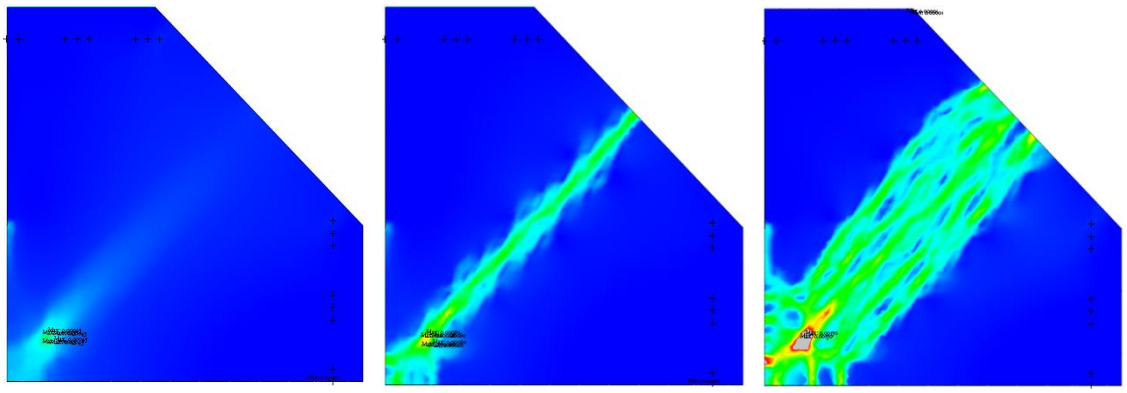

Stage A Stage B Stage C

Figure 4.29 crack patterns in alternative 2 for different load steps.

4.6 Crack band width

As mentioned in chapter 2.3.3, the smeared crack approach with rotating cracks was chosen. The crack band width must then be chosen; it is based on the assumption that one crack will localize in a certain length of the structure; thereby a length scale for the material is introduced. In the present work, three different values were used as crack band widths to study the effect of this parameter. In all the generated models, the element size (mesh size) was 35mm and three different crack band widths with lengths of h_{cr}= 10, 35, 100mm were examined. Changing the crack band widths results in different strain values in the stress versus strain behavior given as input for the material.

$$\varepsilon = \frac{f_{ct}}{E_c} + \frac{w}{h_{cr}} \qquad \textit{Equation 4.1}$$

Figure 4.30 shows the results for different crack band widths; as can be seen, the chosen value of 35 mm gave results that corresponded best to the experimental. Increasing this parameter resulted in lower capacity throughout the entire analysis i.e. in the cracking point, reinforcement's yielding and failure.

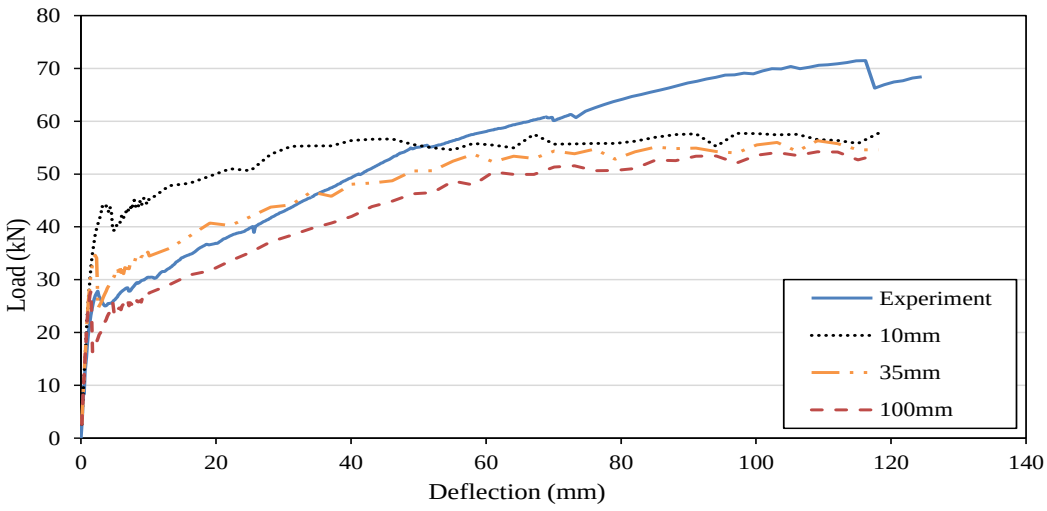

Figure 4.30 Load- deflection diagrams for different choices of crack band widths

4.7 Load

A deformation on the steel plate was defined for the displacement control. Two ways of applying load were investigated in this work:

- Only in one node: Displacement was applied in only one node. Figure 4.31(a).
- Several nodes: Tyings were used in order to have the same displacement in several nodes and not only in one node, see Figure 4.31(b).

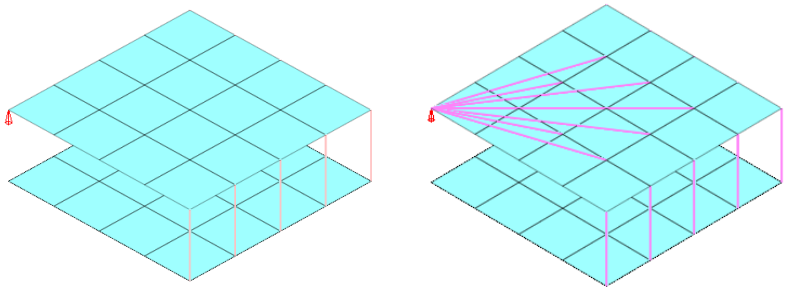

a) Only in one node **b) In several nodes**

Figure 4.31 Different ways of applied load

The results of this investigation showed that the load-displacement diagrams in both of the cases are similar and thus no big influence in the results were observed, see Figure 4.32.

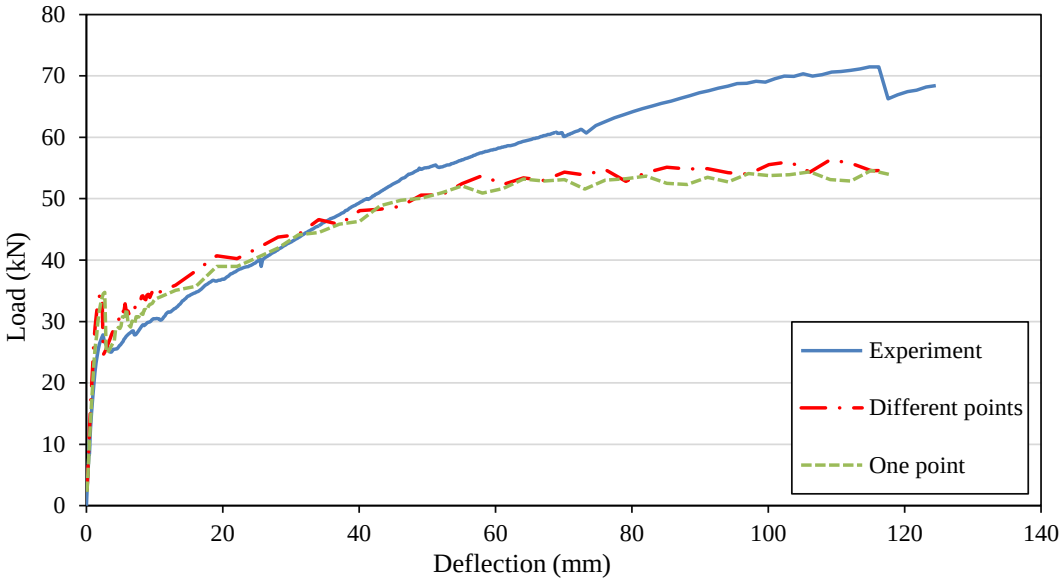

Figure 4.32 Load-displacement results for ways of applying load

4.8 Poisson's ratio

Three analyses were made to investigate the effect of different Poisson's ratios. This parameter was defined as an input data for concrete and as explained in chapter 4.3, the selected Poisson's ratio for the reference model was 0.15 and to observe its effects, two more analyses, one with higher (ν= 0.2) and one with lower (ν= 0.05) values were conducted. The load-displacement diagram in Figure 4.33 indicates that changing Poisson's ratio did not affect the results before cracking, while decreasing Poisson's ratio resulted in higher stiffness in the post cracking stage.

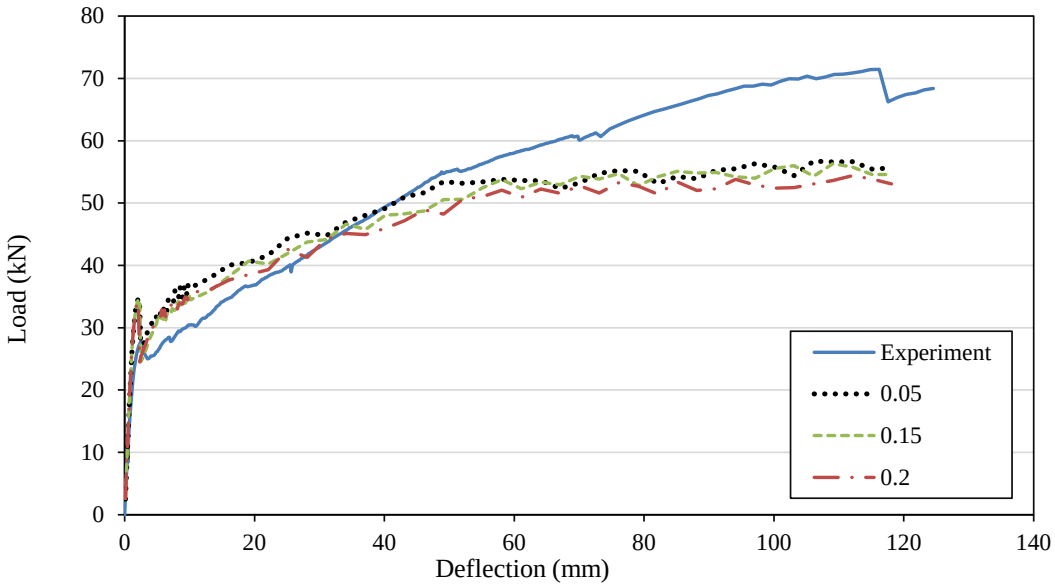

Figure 4.33 Load-deflection results for different Poisson's ratios

4.9 Integration point

As explained in chapter 4.3, the used integration scheme in the plane (surface) was Gauss (Figure 4.34a) and over the thickness was Simpson (Figure 4.34b). In this section, influence of integration points over the thickness was studied. Hence, two models with five and eleven points over the thickness were generated and analyses were performed to compare the results.

a) In-plane integration b) Thickness integration

Figure 4.34 Gauss and Simpson integration scheme, from (TNO Diana, 2009)

As it is shown in Figure 4.35, the results for both of the cases are quite similar. At cracking there was no difference in the results; both models had one integration point at the most tensioned fiber. For intermediate deflections, between ~20-60 mm, the analysis with 5 integration points was slightly stiffer than the analysis with 11 points. This was probably because the analysis with 11 points described the compressed side slightly better, with more than one integration point in the compressive zone, see Figure 4.34b. For larger deflections, the difference was again very small, probably because there was only one integration point in the compressive zone in both analyses.

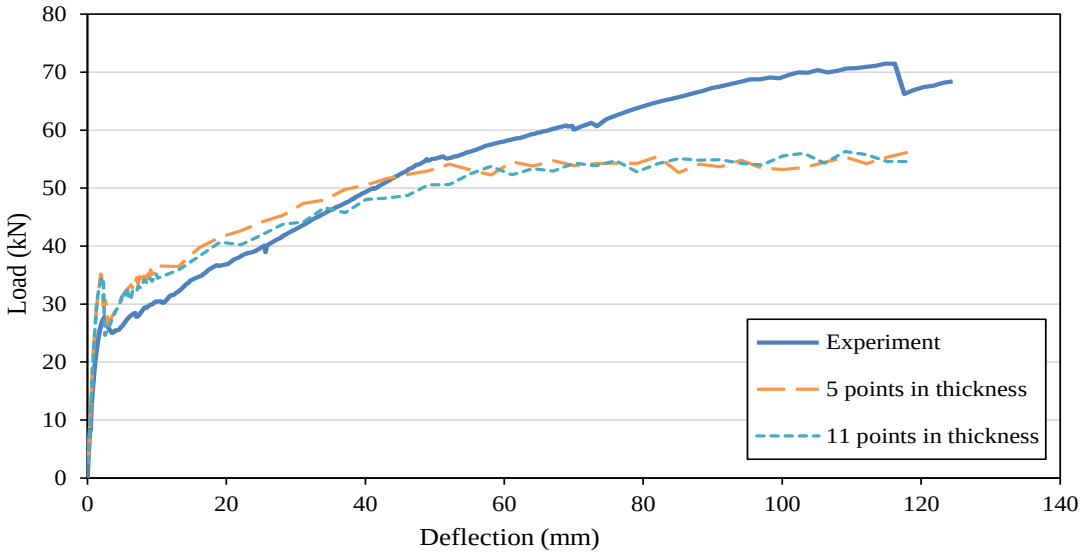

Figure 4.35 Load- deflection results for different integration points

4.10 Different tensile models

As described in chapter 2.3.3, different tensile curves can be used to model the tensile behavior of concrete. Here, six different tensile models were used and the results are presented in Figure 4.36. The only input data that was needed for using constant tensile model was maximum tensile strength of concrete while in linear, Hordijk and exponential models, crack band width and fracture energy were also required. The crack band width was, when required, set to the element size (35mm). The results in the constant model showed a significantly overestimated capacity compared to the experiment because the tensile capacity remains after cracking, which is not reasonable for concrete. The difference in results for the rest of the models was minor, with slightly better agreement to the experimental results for the multi-linear model.

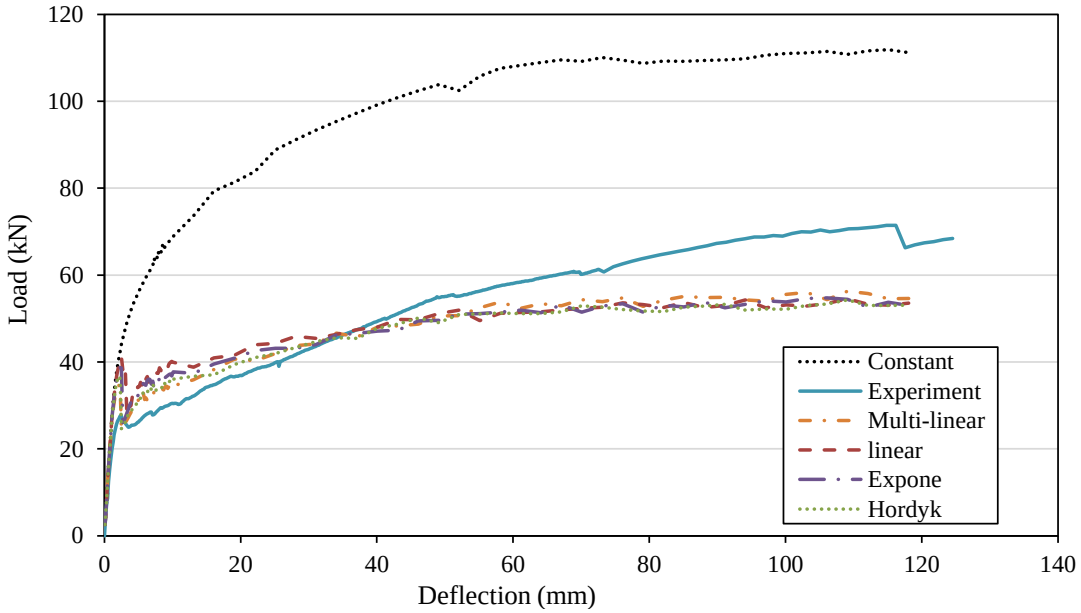

Figure 4.36 Load-deflection diagram for different tensile models

4.11 Steel fiber reinforced slabs

In this section, slabs reinforced with only steel fibers were studied. The material properties and fiber type was described in chapter 3.2.3. Regarding the variation of the material properties, six different samples were tested in the laboratory; see (Rempling, Fall, & Lundgren, 2013). In FE analyses, three alternatives for input data of steel fiber reinforced concrete properties were assumed, based on an average results as well as the two most extreme test specimens (referred to as high and low). Stress-deformation diagrams from the uniaxial tensile tests were translated to stress-strain curves by using Equation 4.1, see Figure 4.37.

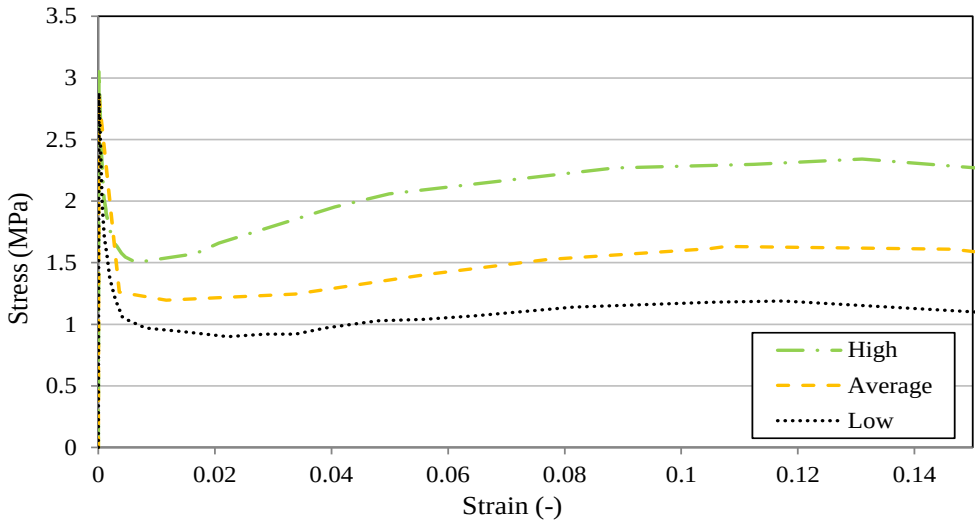

Figure 4.37 Stress-strain diagram for fiber reinforced concrete

Figure 4.38 shows the results from all three analyses compared to experimental results. In all three FE analyses, stiffer behavior was obtained in both pre and post-cracking stages. One possible reason to explain this difference can be that the input comes from notched uniaxial tests; thus the location of the cracks was determined in advance through the placement of the notches, while in the slabs the cracks formed at the weakest spots.

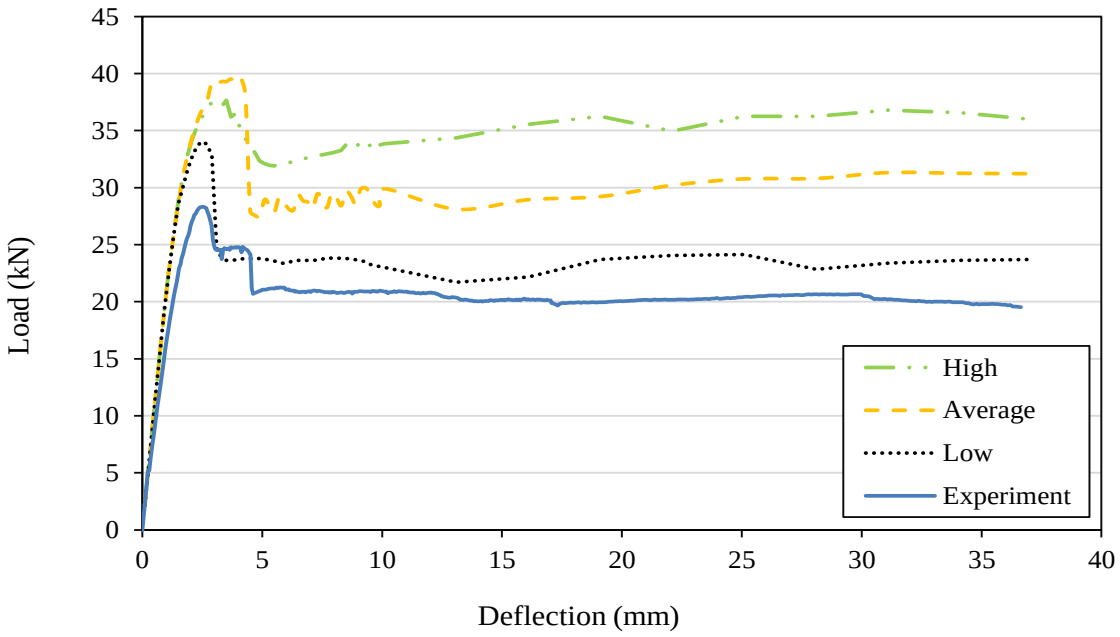

Figure 4.38 Load-deflection results for steel fiber reinforced slabs

Crack patterns for steel fiber reinforced concrete slabs are shown in Figure 4.39 for different deformations in a fixed strain range between 0 and 10^{-3}. In the SFR slabs, the first crack became decisive; the cracks propagated in a line from the most stressed area of the slab, which was under the steel plate (see Figure 4.39a) and it continued towards the free edge (Figure 4.39b). This behavior agrees with the experimental observations.

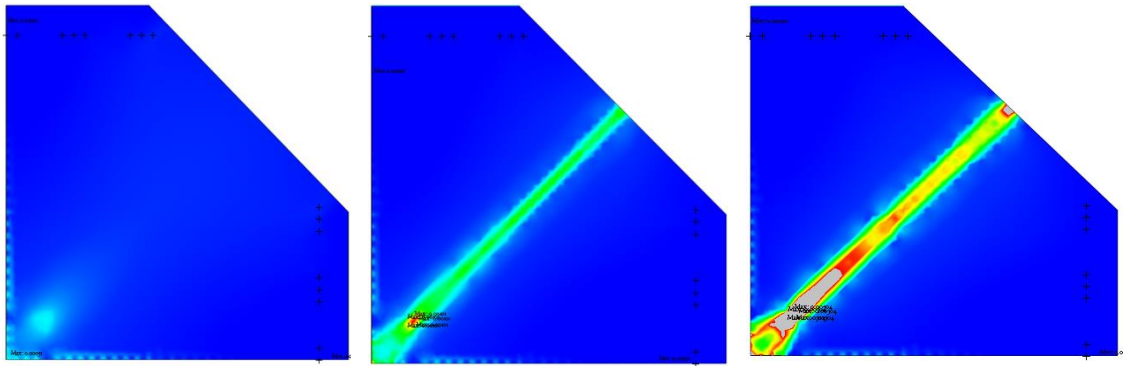

a) 2.1mm **b) 4.5mm** **c) 13.1mm**

Figure 4.39 Crack pattern in reinforced slabs with steel fibers only in related deflection

4.12 Reinforced slabs with both conventional and steel fiber

Reinforced slabs with both steel fibers and conventional steel bars were studied as the last reinforcement alternative in this work. Three different analyses were carried out due to varying material properties for the SFRC which were classified with different residual tensile strengths of high, average and low and as described in chapter 0. The load-deflection diagram is presented in Figure 4.40. The analysis with lowest residual tensile strength gave results close to the experimental at the cracking point but underestimated the post cracking capacity. On the contrary, the analyses with higher residual tensile strengths gave a higher cracking load but better agreement was obtained in the post cracking stage. All three FE analyses overestimated the cracking load and underestimated the stiffness and capacity after cracking.

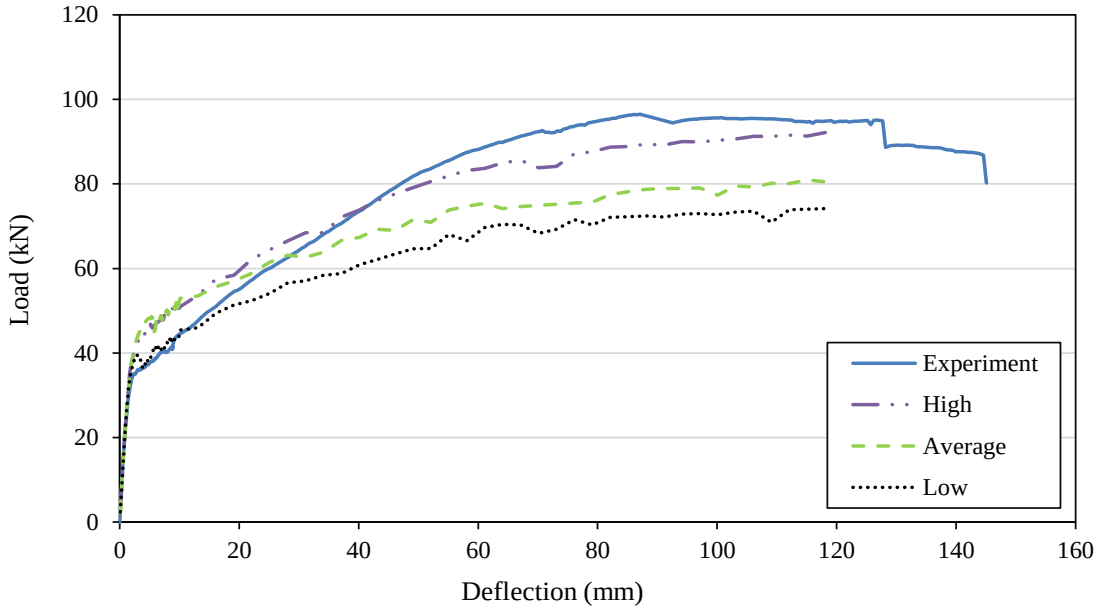

Figure 4.40 Load-deflection results for reinforced conventional and steel fiber slabs

The crack pattern in different steps for slabs with combined reinforcement is shown in Figure 4.41. The results show that larger area of the slab was encompassed by cracks; probably involving points which were not only the weakest, which is a result of combining steel fiber with conventional reinforcement.

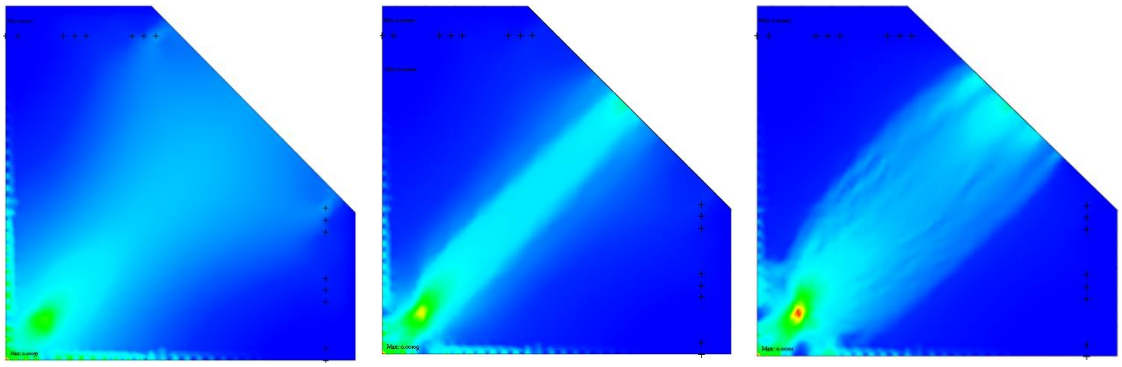

a) 2.1mm **b) 4.5mm** **c) 13.1mm**

Figure 4.41 Crack pattern for combinational reinforced slabs in related deflection

4.13 Discussion

Different modeling choices were studied to investigate their effects on FE analyses of reinforced concrete slabs. The results showed that for all modeling choices (except slabs with steel fibers as only reinforcement), the capacity from cracking until an applied deflection of almost 40mm deflection was overestimated; after that point until failure the capacity was underestimated. One reason for the overestimation from cracking to 40mm deflection could be that fully embedded reinforcement was used, instead of more realistic bond-slip between concrete and reinforcement.

Problems appeared for modelling of the supports. In both strong and weak direction, when the uplift was allowed, more accurate results were obtained in all of the chosen steps comparing to the experiment.

Furthermore, some problems were faced when meshing the slab with quadrilateral elements. It was not possible to mesh the whole models by using only quadrilateral elements; therefore a few triangular elements were also generated. This was time consuming, because integration schemes had to be defined separately in .dat files for both triangular and quadrilateral elements.

It is recommended to investigate the effect of mesh alignment also for quadrilateral elements; the analysis with triangular elements didn't show any major effect of the mesh alignment but it is suspected that this effect would be larger for quadrilateral elements. For the mesh density investigations, long time was needed to run the analyses with denser mesh (approximately 2 days for the model with half and almost 6 days when the mesh size was equal to a quarter of the reference mesh size).

One interesting note was that while using steel fibers as the only reinforcement, the capacity was overestimated at all stages of loading while in the analysis with both conventional and steel fiber reinforcement, the capacity was underestimated. One reason for this difference could be that in the slabs with fibers only, the first crack becomes decisive; the location of that is probably governed by the weakest points. While in the slabs with combined reinforcement, several cracks formed; involving points which were not only the weakest ones.

5 Conclusions

Evaluations of different modeling choices revealed that some of them such as mesh density, different tensile models for concrete, crack band width and reinforcement types had major effects on analyses. On the other hand, some of the modeling choices did not affect, or had only a minor effect on the results, like mesh type, mesh alignment, Poisson's ratio, modeling of the applied load and number of integration points over the height.

Results from the effect of different mesh densities showed that in all of the studied alternatives, stiffer behavior just after cracking but underestimated response after yielding until failure were obtained compared to the experiment. In FE analyses, when the crack band width was chosen to be the same as the element size, denser meshed models resulted in significantly stiffer behavior and by increasing the mesh size, less stiff behavior in all of stages was seen. While, in the models with a constant crack band width, similar results were achieved by changing mesh densities. Thus, crack band width had an important role in the modelling. Furthermore, as can be expected, the models with denser mesh consumed longer computation time compared to the coarser meshed models.

Different tensile models for concrete were used. Very similar results were obtained for all of the tensile models used except for the constant model, which significantly overestimated the stiffness and capacity. This agrees with what could be expected for a brittle material as concrete.

Adding fibers improved the post-cracking response since it increased the ductility of the material. By comparing the two types of slabs, one with only steel fiber and the other one with combination of steel fiber and conventional reinforcement, these remarks can be pointed out: In the slab reinforced with steel fiber only, the capacity was overestimated in the analysis, and a concentrated crack pattern was formed. While for slabs with combined reinforcement, the cracking load was higher and the load from yielding until failure was lower in the analysis compared to experiments.

The number of integration points over the thickness was increased to study the influence of this parameter. Similar results were obtained for both of the cases probably because in both of the analyses, there was at least one point to describe the compressive zone. For larger deflections, the difference is again very small, probably because there was only one integration point in the compressive zone in both analyses.

6 References

Akin, J. (2009). *Finite Element Analysis Concepts* . Houston, Texas : Rice University, Houston, Texas .

Bayasi, Z. a. (1989). *Use of Small-Diameter Polypropylene fibers in Cement based materials.*

Bekaert. (n.d.). Retrieved from Bekaert. (2012, June 18). http://www.bekaert.com/. Retrieved May 17, 2013, from http://www.bekaert.com/en/Product%20Catalog/Products/D/Dramix%205D%20steel%20fibers%20for%20concrete%20reinforcement.aspx.

Blanco, A. (2013). *Characterization and modelling of SFRC element.* Barcelona: Universitat Politècnica de Catalunya.

CEN. (2004). *Design of the concrete structures.* Brussels: European commitee for standardisation.

Cook, Malkus, & Plesha. (1989). *Concepts and Applications of Finite Element Analysis.* John Wiley & Sons.

Daniel, J. R. (1998). *Fiber reinforced Concrete.*

Ericsson, F. (2010). *Punching Shear in Reinforced Concrete Slabs Supported on Edge Steel Columns.* Göteborg: CHALMERS UNIVERSITY OF TECHNOLOGY.

Fall, Rempling, & Lundgren. (2013). Experiments on fibre reinforced concrete two-way slabs. *7th International Conference: Fibre Concrete.* Prague, the Czech Republic: ISBN 978-80-01-05239-6.

Glavind, M. (1992). *Evaluation of the Compressive Behaviour of Fibre Reinforced High Strength.* Technical University of Denmark, Department of Structural Engineering.

Grünewald, S. L. (2011). *Improved tensile performance with fibre reinforced self-compacting concrete* .

Hand, F.R., Pecknold, D.A. and Schnobrich, W.C. (1973). Nonlinear Layered Analysis of RC Plates and. *Journal of Structural Division, ASCE*, Vol. 99, No. ST7, pp. 1491-1505.

Helen Broo, Karin Lundgren, Mario Plos. (2008). *A guide to non-linear finite element modelling of shear and torsion in concrete bridges.* Göteborg: Department of Civil and Enviromental Engineering Chalmers University of Technology.

Hyo-Gyoung, Filip Filppou. (1990). *Finite element analysis of Reinforced Concrete structures under Monotonic Loads.* Berekley, California: University Of California.

Jansson. (2008). *Fibres in reinforced concrete structures - analysis, experiments and design.* Gothenburg.

Jansson. (2011). *Effects of Steel Fibers on Cracking in Reinforced Concrete.* Division of Structural Engineering, Department of Civil and Environmental Engineering. Göteborg: Chalmers University of Technology.

Kansarav, K. (2004). *Development of Membrane, Plate and Flat Shell Elements in Java.* Blacksburg, Virginia: Virginia Polytechnic Institute & State University.

Kwak, C. F. (1990). *Finite element analysis of reinforced concrete structures under monotonic loads.* . California, Berkeley : Department of Civil Engineering University of California.

Lin, C.S. and Scordelis, A.C. (1975). Nonlinear Analysis of RC Shells of General Form. *Journal of Structural*, 523-538.

Löfgren, I. (2005). *Fibre-reinforced concrete for industrial construction.* Göteborg, Sweden.: Department of Civil and Environmental Engineering, Structural Engineering, Chalmers University of technology.

Plos, M. (1996). *Finite element analysis of reinforced concrete structures.* Gothenburg: Chalmers Universuty.

Rempling, Fall, & Lundgren. (2013). *Results from tree point bending and uni-axial tension tests.* Prag: 7th International Conference 2013.

TNO Diana. (2009). *tnodiana.com.* Retrieved from https://support.tnodiana.com/manuals/d93/Diana.html

Yang, Saigal, & Liaw. (1990). *Advances of Thin Shell Finite Elements and some applications,* Pittsburgh, Department of Mechanical Engineering, Carnegie Mellon University.